STUDIES OF BASIC ELECTRONIC PROPERTIES
OF CdTe-BASED SOLAR CELLS & THEIR EVOLUTION
DURING PROCESSING & STRESS

Annual Technical Report, Phase 2

October 15, 2002 – October 15, 2003

SUBCONTRACT NO. ADJ-2-30630-05

UNDER

PRIME CONTRACT NO. DE-AC36-99-GO10337

V.I. Kaydanov, T.R. Ohno

Colorado School of Mines
Golden, CO 80401

Contract Technical Monitor: Kenneth Zweibel

NOTICE

PREFACE

This project, "Studies of Basic Electronic Properties of CdTe-Based Solar Cells & Their Evolution During Processing & Stressing", which is performed at the Colorado School of Mines (CSM), is part of the NREL Thin-Film Partnership Program. The project addresses long-term research and development issues related to polycrystalline thin-film solar cells. Our general research approach is based on combining activities aimed at improvement of cell performance and stability with activities aimed at increasing our fundamental understanding of the properties of materials making up the cells: CdTe, CdS, multi-layer back contact, and transparent conducting oxide (TCO) front contact. We emphasize the relation between composition, structural and electronic material properties and various processing procedures as well as the microscopic mechanisms responsible for the cell performance and its degradation.

There is a lack of knowledge and understanding of basic issues behind the CdTe/CdS cells performance and stability, such as the nature and electronic properties of impurities and defects that control the majority carrier concentration, mechanisms of the dopant compensation, recombination processes, their nature and properties, migration and transformation of defects under various processing, stress, and operating conditions, etc. We believe that better basic understanding of the specific influence of grain boundaries, especially for fine-grain materials like those making up CdTe-based cells, is now one of the most important issues we must address. We need to clarify the role of grain boundaries (GB) in forming the film electronic properties as well as those of the p-n junction. It is important to study and understand the influence of the GB boundaries on the spatial distribution and migration of impurities and electrically active defects. To fulfill these tasks one needs to develop new methods and techniques (or adjust existing ones) for material characterization as well as more sophisticated approaches to the data analysis and modeling. This report presents studies relevant to the problems formulated above that were carried out at CSM at Phase II of the Project according to the Statement of Work and Tasks of the Subcontract.

Section 1 presents the results of our studies of electroluminescence (EL) that demonstrate high sensitivity of the EL intensity and its spatial distribution (micro non-uniformities) to the cell processing/composition and stressing at various conditions. Many of obtained data on EL in conjunction with photoluminescence (PL) and J-V characterization, pointed out on the

nonuniform back contact as a major source of nonuniformity in injection level and EL intensity. This concept was confirmed experimentally by the study of the cells with intentionally introduced lateral nonuniformity by means of nonuniform Cu doping. New equipment allowed high spatial resolution two-dimensional imaging of integrated EL and PL intensity as well as one-dimensional scans of the spectrally resolved luminescence. EL and PL images are obtained from the same area of a cell. Comparison of EL and PL spectra and spatial intensity distribution along with the LBIC images of the same cells obtained at CSU, provided new opportunities to study mechanisms of nonuniformity. In particular, luminescence spectra demonstrate several defect-related transitions lower than the band gap energy. The spatial distribution of intensity is energy dependent and is effected by nonuniform doping.

Section 2 presents studies of deep electronic states (traps) in CdTe absorber layer. In this Phase we have significantly broadened our technical capabilities. A new measurement system was developed that allow us to measure frequency- and bias-dependent admittance in a wide range of temperature. In addition, we can make measurements of the long transients (up to tens of hours) at a fixed temperature. In this section we briefly discuss the basics of admittance spectroscopy (AS) and the information obtained with this method on deep states in CdTe. We discuss errors of common approaches to AS (and DLTS) data analysis due to the high trap concentration revealed for all thin film CdTe cells. In particular, trap concentration is underestimated while the doping level derived from C-V measurements can be strongly overerestimated. Other problems related to detection and studying deep states, especially very slow ones, are discussed along with some new (at least for CdTe) approaches to their solution. The section is concluded with a brief description of the parameters and options provided by this new measurement system, the first results of measurements, focused mostly on transients and information on deep/slow states already derived from them.

Studies of CdTe/ZnTe interface with scanning tunneling microscopy (STM) are presented in Sec.3. In this Phase we have significantly modified techniques of measurements which provided new opportunities in mapping and studying of electrical properties of the back contact. A novel technique, charge injection spectroscopy (CIS) in an STM, provides detailed maps of carrier transport near the interface. The lateral resolution below 20 nm is about two orders of magnitude below the CdTe grain size. It was shown that charge transfer between p^+-ZnTe and p-CdTe is highly nonuniform, demonstrating large areas with roughly constant high contact

4

resistance coexistent with nanoscale high conductance pathways. A majority of the cell current flows along these pathways, which are often localized at grain boundaries. This may indicate a possible role of grain boundaries as efficient transport channels, at least for the ZnTe:Cu/metal back contact. Conducting paths found within a few of the grains suggest specific intragrain defect also may cause lowering of the contact resistance.

We have also worked upon further developing of the near-field scanning optical microscopy (NSOM). First high resolution maps of the photocurrent collection in plan view were obtained from CdTe/CdS cells of a substrate configuration prepared by the University of Toledo. Considerable contrast is seen between the grain bulk and grain boundary regions. These are only preliminary results, therefore they are not presented in this report.

In this Phase we have improved deposition procedures with gas jet deposition (GJD) and electrodeposition (ED) techniques. For GJD the optimum deposition conditions given our limitations on sample heating has been obtained and reported in previous quarterlies. We have examined the effects of buffer layers and show some device improvement. In ED we have changed the system to increase deposition rates, but still are working on device performance. We will present these accomplishments later in our following Quarterly and Final Reports after obtaining more reproducible, statistically representative results and better understanding of perspectives and directions of further optimization of processing technology.

Table of Contents

List of Figures

List of Tables

1. ELECTROLUMINESCENCE IN CdTe/CdS SOLAR CELLS

1.1 Introduction

Our previous studies [1] indicated that CdTe/CdS cells emitted light under forward bias in the photon energy range in the vicinity of the CdTe bandgap. Electroluminescence (EL) was observed at room temperature as well as at T~15 K. Though the excitation mechanism is different, EL is similar to the more commonly employed photoluminescence (PL) characterization technique. The principal difference is that excess electron-hole pairs are injected electrically instead of optically. Their recombination produces luminescence. The intensity of EL emission is roughly proportional to the product of the electron and hole concentrations. Because n-CdS is believed to be doped heavier than the p-CdTe absorber layer, the $n \times p$ product reaches a maximum in the CdTe near the junction and this is the region where EL originates. EL spectra have been found to be similar to PL spectra in CdTe [1]. The same was found previously for many other materials, for example, for SrS:Cu and SrS:Ag, Cu, Ga thin films [2], Si^+-implanted SiO_2 [3], CdS nanocrystals [4], and $Si_{1-x}Ge_x$ alloys [5]. However, few studies of EL in CdTe/CdS cells are known whereas studies of PL are numerous. Our intensive EL studies are not intended to replace PL. The similarity of the spectra observed along with difference in the mechanisms and techniques of excitation, lends further credence to the usefulness of EL and PL as complementary techniques and the ability to use information from one to explain effects in the other.

One inherent property solar cells based on polycrystalline thin films is nonuniformity of the photo-electronic properties in various spatial scales. It is obvious that macro-nonuniformities reduce the efficiency of solar modules. Recently it was shown (Karpov, Shvidka, Compaan, et.al, [6]) that a single micro-nonuniformity, e.g. small area region of reduced open circuit voltage, can significantly affect the performance of the whole cell. Standard characterization techniques such as current-voltage, capacitance-voltage, and quantum efficiency measurements average properties over the area of a solar cell and do not detect micro-nonuniformities. Contrasting these methods is a new wave of spatially resolved characterization tools such as cathodoluminescence (CL) [7], electron beam induced current (EBIC) [8,9], laser beam induced

current (LBIC) [4], near-field scanning optical microscopy (NSOM) [11], PL mapping [12], and, finally, the spatially resolved electroluminescence, discussed here.

There are several advantages making EL attractive as a characterization tool. Though our EL technique (described below) does not have the highest spatial resolution among the techniques listed above, the spatial dynamic range of resolved EL data may be the greatest, with a linear resolution of several microns to scans of over a centimeter. Also, unlike other methods that usually involve high injection rates, the degree of excitation required to induce measurable EL could be on the order of J_{sc} or even less. In other words, the conditions that produce EL are comparable to the conditions of a device in normal operation. This moderate excitation level increases confidence that the observed EL patterns can be related to cell performance. Furthermore, low injection ensures that characterization will not degrade device performance (as verified by I-V data taken before and after EL imaging). As a final point, EL is technically simple to perform as it can be observed at room temperature, and data acquisition is relatively quick. Because it is simple to implement, EL may find use as a standard production monitoring tool in an industrial application.

Below we describe the techniques for EL measurement/imaging and the data treatment procedures we have developed and used in these studies. Then, some selected results are presented of experimental studies of EL to demonstrate the sensitivity of EL to the processing procedures, composition, and stressing. The studies were performed on the cells manufactured with various deposition techniques at different facilities: vapor transport, First Solar, LLC (FS); close-space sublimation, University of South Florida (USF) and Colorado State University (CSU); sputtering, University of Toledo (UT). Besides, some cells were made using the FS CdTe/CdS material with the back contact applied at our facilities (FS/CSM). One of the most and common features of the EL images is non-uniformity of the EL intensity. The patterns of bright spots vary with processing procedure and stressing. A significant portion of this section is devoted to clarification of the mechanism of nonuniformity: what processes and in what parts of a cell are responsible for and define the structure of the EL patterns. Because electroluminescence originates from recombination of excess carriers injected into p-n junction region by current, the nonuniformity in EL intensity may be dominated by either by the nonuniformity in concentration of non-radiative recombination centers or by nonuniformity in the injection level.

1.2   Technical

The forward biasing used to induce EL is provided by a Keithley 2120 3A SourceMeter$^®$ operating as a current source. This device also allows for I-V curves to be measured without moving the cell from the EL apparatus. EL images are acquired with a Santa Barbara Instrument Group ST-5C cooled CCD camera that has a 320×240 array of 10×10 μm^2 square pixels. The cell is mounted on a micrometer-controlled stage and imaged through either a 1.3× or 10× microscope objective . The 10× objective allows for resolution on the order of the optical limit for the infra-red EL, namely several microns. The 1.3× lens images a 1.6×1.2 mm^2 rectangular area of a cell. Multiple images can then be stitched together graphically to form a composite of the entire cell (Fig. 1.1). Cells to be compared are imaged at constant current density as noted below, and standard CCD acquisition time is 60 seconds for all data shown.

Comparison of the low-resolution image of the UT cell in Fig.1.1 to the highly magnified image of the same cell in Fig. 1.2 reveals non-uniformity on different scales.
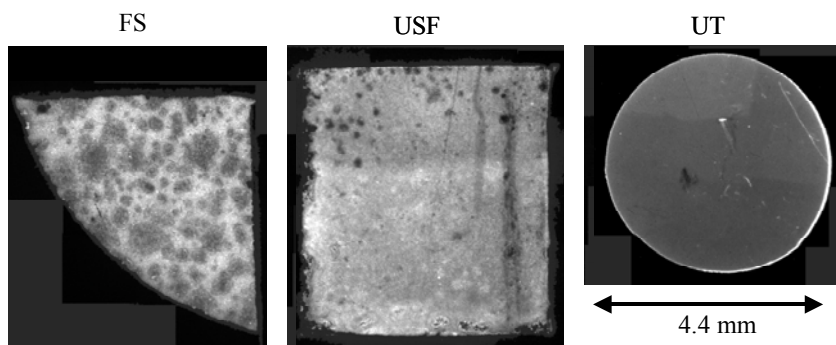
Figure 1.1   Composite, low magnification EL images.
All images have the same scale in dimensions but not brightness. Differences in total EL intensity did not exceed ~30 %. Note, the FS cell was scribed from a circle into a sector to approximate the area of the UT cell while still showing the edge of the original cell. Current density $\cong$ 33 mA/cm^2 for all images.
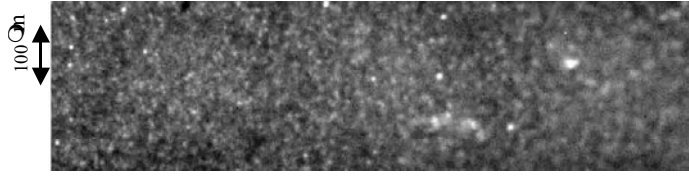
Figure 1.2. High magnification image of UT cell shown in Fig. 1.1 above. Current density $\cong$ 33 mA/cm^2

Image data is numerical, consisting of a 320×240 array of numbers with each number representing the photon count at each pixel. The simplest piece of information that can be drawn from this data is the mean EL intensity. Often the EL emission is concentrated in small bright spots. The brightness and the number of spots increases with increasing injection current levels (Fig. 1.3). Irreversible changes in EL were observed with current density in excess of 1A/cm^2. Currents below this threshold applied for periods less than an hour did not appear to change the EL images.

J = 20 mA/cm^2 J = 90 mA/cm^2 J = 190 mA/cm^2
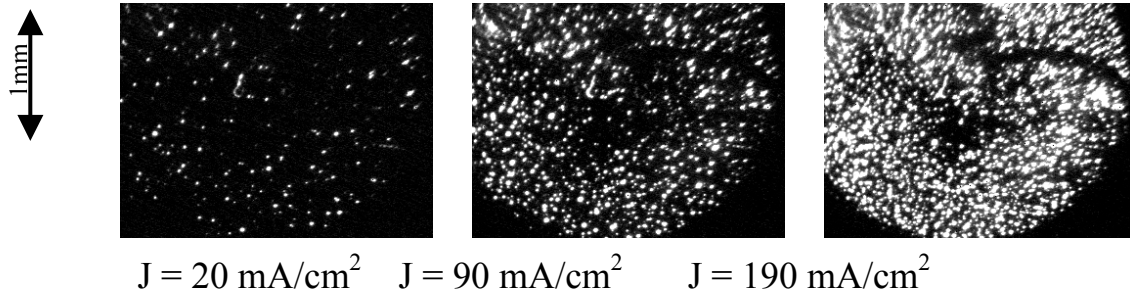
Fig. 1.3. EL changes with current

Exploiting the spatially resolved nature of the measurement allows one to characterize quantitatively the non-uniformity in the EL emission. A simple parameter called the "non-uniformity" is defined as the standard deviation of EL intensity normalized by the mean EL intensity. Generally, trends in this parameter mirror qualitative observations made from the CCD images. Selected histograms in Fig.1.4 make differences in EL non-uniformity more visible.

Note how the low magnification UT image has the narrowest histogram (indicating that it is the most uniform), whereas the FS histogram is significantly wider. The difference in width and

shape of the low and high magnification UT histograms is indicative of the small-scale non-uniformity. The FS histogram has a peak with a shoulder, indicating two separate populations.
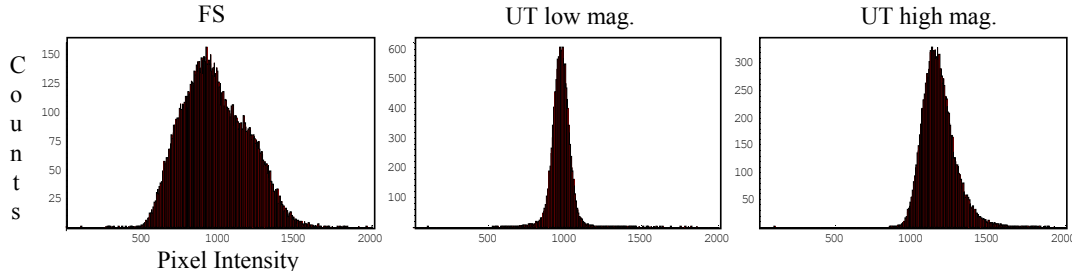
Figure 1.4. Selected Histograms. FS cell - low magnification, UT- low and high magnification

The differences between the low- and high-magnification image histograms for the UT cell indicate that there coexist several characteristic non-uniformity spatial scales. To detect and study them we have started to use variogram analysis which is a geostatistical technique used to quantify the spatial correlation of data [13]. The extent of this spatial correlation helps to quantify the scale and possible anisotropy in the non-uniformity structures underlying electroluminescence. For example, correlation feature sizes of ~10 μm and ~60 μm were found in the UT cells.

Recently we have introduced new instrumentation to allow high spatial-resolution imaging of luminescence with *spectroscopic measurements* on the same length scale. This was intended to complement our existing system based on a Santa Barbara Instrument Group ST-5C CCD camera. The new instrument is a Princeton Instruments Spec-10:100BR Digital CCD Spectroscopy System with liquid nitrogen-cooled, back-illuminated, deep-depletion CCD camera (1340 x 100 pixels with 20 x 20μm pixels). The monochromator/spectrograph is capable of operation in a two-dimensional imaging mode or a one-dimensional spatial mode with spectroscopic data. Because of the increased sensitivity of the CCD, data can be acquired much more rapidly at lower levels of injection. The spectrometer optics limits magnification. The 20 μm pixels place a limit on the spatial resolution of ~ 10 μm using slightly magnifying optics at the input. Another feature of the high sensitivity is that we can change the excitation source from injected current to a low powered laser such as a He-Ne laser to perform PL on the same cell used for EL measurements. The maps of EL and PL can be obtained from the same fragment of

the cell area providing the opportunity to compare the spatial distribution of intensity and the emission spectra of EL and PL. Results obtained with this system will be discussed in more detail below.

1.3 Results of Experimental Studies of EL on CdTe/CdS Solar Cells

Here we focus on variation in EL emission due to variation in deposition technique, postdeposition treatment, doping, back contact application procedure, and stressing.

Fig. 1.1 visibly demonstrates differences in the EL images for the cells manufactured at different facilities with different deposition techniques: vapor transport deposition (FS), close-space sublimation (USF) and sputtering (UT). The most nonuniform seems to be the FS image, while the UT one is seemingly the most uniform. However images obtained at higher magnification (Fig. 1.2) reveal nonuniformity in the latter. In spite of significant differences in the EL patterns the EL intensity averaged over the cell area (mean intensity) does not vary considerably from cell to cell. At the same time the mean EL intensity from the CSU cells (close space sublimation) was several times lower than for the cells presented in Fig. 1.1.

To examine the influence of the postdeposition $CdCl_2$ treatment, a study was conducted using FS/CSM cells: the FS CdTe/CdS structures with back contacts (ZnTe:Cu/Au) processed at the Colorado School of Mines. EL from cells that underwent $CdCl_2$ treatment was compared to EL from nominally identical cells without $CdCl_2$ treatment.
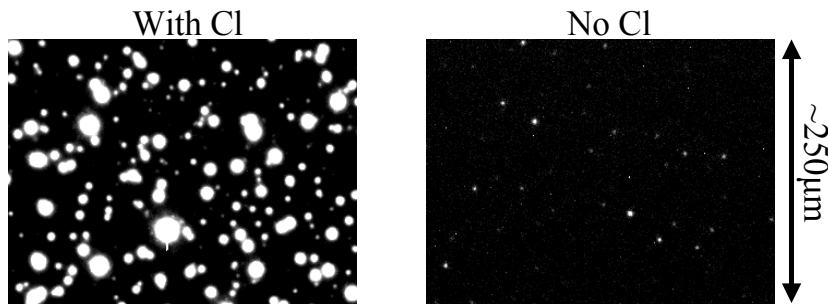
Fig. 1.5. Effects of $CdCl_2$ treatment on EL. Current density $\cong 50$ mA/cm^2.

Both sets of cells showed isolated bright spots less than 20 microns in size surrounded by a dark background with an emission that was indistinguishable from the dark counts (Fig. 1.5). The cells with Cl had more bright spots, and spot intensity was greater. Furthermore, the rate of increase of EL intensity with current was lower in the cells without Cl. Drive level capacitance profiling (DLCP) was also used to estimate the deep level density in these cells [14]. It was found that the cells subjected to the Cl treatment (high efficiency) possessed more traps than the cells without $CdCl_2$ treatment (much less efficient). This result was unexpected, as a greater trap concentration would supposedly imply less luminescent recombination, but is important nonetheless because it proves that effects of Cl treatment (a crucial step for producing efficient CdTe devices) can be monitored with EL.

Influence of the Cu dopant on EL intensity was studied on the cells fabricated at CSU processed with different duration of Cu vapor deposition: 0, 0.5, 1.0, and 4.0 minutes. There was a noticeable change in EL (both in intensity and pattern) due to the presence and amount of Cu. The most brightly emitting cells were those of 0.5 and 1 min. of Cu deposition. These cells also demonstrated the most nonuniform EL intensity. Compared to these two processing conditions, 4 min. of Cu led to a small decrease in emission intensity (less than a factor of 2) as well as an increase in uniformity. The cells without Cu showed a ~4x decrease in emission intensity and also slightly increased uniformity compared to those cells with Cu.

Influence of the back contacting procedure is demonstrated in Fig. 1.6. Two sets of cells were fabricated on First Soar material with the Cu/ZnTe/Au back contacts applied at CSM. The difference between the two was in the thickness of ZnTe and amount of Cu.

(a)   (b)
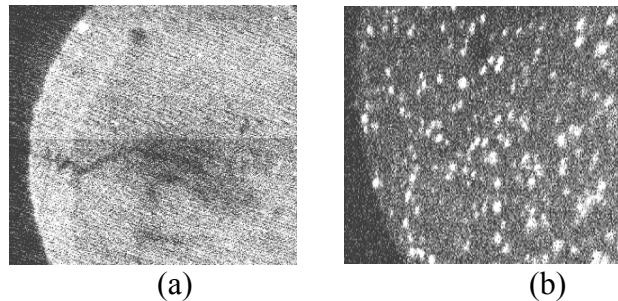
Figure 1.6   EL changes with back contact variation
(a) 11 Å Cu and 500 Å ZnTe deposited;   (b) 8 Å Cu and 850 Å ZnTe deposited

The differences in the EL images are obvious. EL in the left image is rather uniform. The bright spots are not seen here, whereas the right one demonstrates them clearly. Also, the mean

EL intensity is higher for the left cell. For the further discussions it seems useful to notice that in the left picture the ZnTe layer is thinner, while the amount of Cu is higher, so that the Cu to ZnTe ratio is 2.3 times greater. Since EL intensity is very sensitive to the back contact as discussed below, this suggests EL can be used as a diagnostic of contact formation and degradation.

One of the most interesting results of stressing was a significant drop in EL mean intensity observed even for "gentle" stress conditions when the cell efficiency did not degrade considerably or did not degrade at all. A similar effect was also observed in [15]. This drop in emission intensity is usually accompanied by an increase in non-uniformity. These great changes in the short term suggest that EL can perhaps be used as an early warning system for detecting cells that are likely to degrade quickly.

A more dramatic stress effect has been seen on First Solar cells, namely the change from a mottled, but relatively uniform EL emission pattern to emission coming only from isolated spots (Fig.1.7). This effect occurred in cells light soaked at V_{oc} for 56 days as well as in cells stressed in light for only 7 days at either V_{oc} or –2V reverse bias.
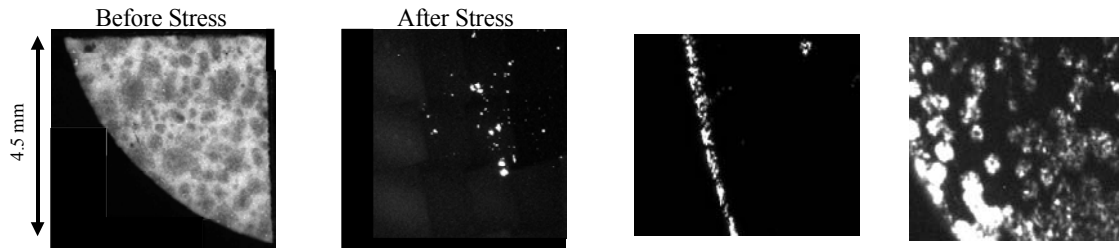
Fig.1.7. EL images for FS cells. Current density $\cong$ 33 mA/cm^2
From left to right: as-prepared; 56 days light soaking; 7days stress at reverse bias;
7 days stress at open circuit; 7 days light soaking.

The following tables summarize results for unstressed and stressed samples. Some data in Table I were also presented in the Phase I (2002) Annual report.

Table 1.1 EL intensity measured with injected current density $J = 600$ mA/cm^2.
The unstressed UT sample showed some contact damage.
Stress conditions: 4 weeks at 65°C, light, open circuit.

Cell	Stressed?	Eff %	Jsc mA/cm^2	Voc V	FF %	EL Mean Count	EL St Dev. Count	Nonuniformity St.Dev./Mean
CSU No Cu	no	4.5	15.3	0.66	44	631	94	0.126
CSU 0.5 min Cu	no	9.7	18.9	0.75	68	3417	465	0.132
CSU 1 min Cu	no	9.7	18.5	0.75	70	2649	322	0.115
CSU 4 min Cu	no	9.3	19.8	0.75	62	2547	265	0.097
CSU No Cu	yes	0.8	6.52	0.59	20	622	76	0.092
CSU 0.5 min Cu	yes	5.9	19.5	0.74	41	3153	505	0.156
CSU 1 min Cu	yes	7.9	19.1	0.74	55	3483	644	0.188
CSU 4 min Cu	yes	10	20.1	0.74	70	2005	343	0.166
FS w/UT contact	no	10	19.2	0.8	67	18150	2856	0.159
FS w/UT contact	yes	8.2	17	0.77	62	5844	1190	0.211
UT sputtered	no	3	17.8	0.56	30	16814	2856	0.157
UT sputtered	yes	4.7	17.3	0.69	39	7974	1190	0.204

The most notable difference between cells prepared with different growth methods was a significantly lower mean intensity of the CSU grown material, as noted previously. In addition stress usually resulted in about 3× reduction in EL mean intensity, while this was not the case for the CSU material. A less certain conclusion for these moderately stressed samples was a small but apparent increase in non-uniformity.

In order to further study this effect, a more severely-stressed set was used in the second investigation for the Non-Uniformity subteam. Unstressed images were reported in the January 2003 quarterly and stressed images were presented at the Summer 2003 CdTe team meeting.

The table below lists figures of merit for the normal cell performance parameters and EL. This set again shows reductions in mean EL emission with stress, ranging from 2 to 7× (no CSU cells were measured in this set, and those tested started with similar initial values).

Table 1.2 EL intensity measured with injection current density J ∼ 33 mA/cm^2.

Current density for USF cells is less certain due to ragged area. Stressed UT20 had a damaged contact, but was included for completeness.

Cell	Stressed?	Eff %	Jsc Ma/cm^2	Voc V	FF %	EL Mean Count	EL St. Dev. Count	Nonuniformity St Dev/Mean
FS17	no	10.7	19.7	0.83	65.7	1027	210	0.227
FS17	yes	5.4	15.9	0.64	57.6	133	104	3.39
FS16	no	9.1	17.4	0.83	63.2	1177	238	0.221
FS16	yes	5.2	13.6	0.66	53	135	185	5.43
USF9	no	18.4	37.1	0.84	59.2	1084	279	0.280
USF9	yes	12.0	29.4	0.75	51.9	260	72	0.452
USF11	no	12.1	35.9	0.84	40.4	805	107	0.154
USF11	yes	9.9	25.1	0.75	50.1	415	91	0.289
UT20	no	12.8	23.4	0.83	65.7	942	98	0.112
UT20	yes	0.4	15.1	0.1	24.7	227	46	0.368
UT26	no	11.1	22.4	0.83	59.4	972	94	0.108
UT26	yes	8.05	17.7	0.75	60.7	187	75	0.863

Now we are able to more conclusively state that non-uniformity increased with stress, with changes that range from 2 to 15 times. Comparison with similar (but not the same) samples measured with other spatially-resolved techniques such as photoluminescence (PL) at the University of Toledo or photocurrent mapping at CSU did not show clear correlations. Thermography matched better, showing an increase in mean value of temperature and increased non-uniformity with stress, as well as occasional 'rings' on the contact edge [16]. Higher temperatures for stressed cells with lower EL emission seems reasonable, as more non-radiative

recombination may have occurred. Probably both EL and thermography nonuniformity reflects nonuniformity in the current flow.

The most pronounced change in non-uniformity was for the FS samples. The I-V dark curves for these cells provide evidence of dramatic change in the cell electric parameters. Figure 1 shows increased rollover, suggesting an increased series resistance, likely due to a back contact diode. Later we will show that the increased nonuniformity in EL is at least partially caused by the non-uniform degradation of the back contact.
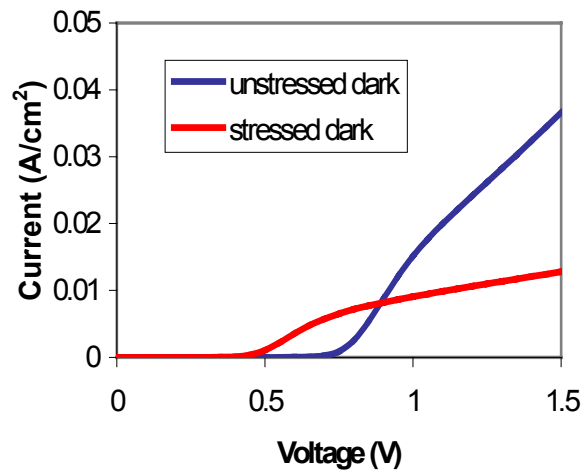
Figure 1.8. First Solar sample from Table 1.2 shows lumped results of stressing.

1.4   Mechanism/s behind EL non-uniformity

In previous sections we have demonstrated EL intensity nonuniformity and its relationship to processing and stressing. The degree of non-uniformity, as well as the patterns of bright spots, vary with deposition techniques, postdeposition treatments, Cu content, back contact structure and properties. The most significant changes in EL intensity and patterns were observed resulting from stressing. The important unresolved question still remains: what mechanisms/processes and in which parts of a cell are responsible for the EL nonuniformity and its changes? In the first place we must clarify the problem what dominates the EL nonuniformity: nonuniformity in the radiative quality of p-n junction or nonuniform injection rate of excess

carriers. The major cause for the first mechanism could be the spatially nonuniform density of recombination centers/defects. For the latter it is nonuniform current density. We will start our discussion with the second mechanism.

1.4.1. Nonuniform current density as a cause for nonuniform EL. Role of back contact

The voltage V across the cell is uniform over the cell area, because high conductance TCO front contact and back contact metallization both are nearly constant potential surfaces. Thus the local current density j is inversely proportional to the local "area resistivity" ρ_a (resistance per unit area of a cell): $j = V / \rho_a$. Brighter EL areas should correspond to higher j (lower ρ_a) local values. One of our experiments verified these expectations. In the stressed FS cell with a very strong EL non-uniformity we have separated (cut) some cell interior fragments that looked rather dark in the whole cell images. Then, the EL intensity was measured (imaged) along with the $J - V$ dependence in dark for the same forward current/area ratio as previously for the whole cell. The resistance per unit area at forward bias, ρ_{fb}, was found considerably higher for the separated fragment than for the whole cell. That means that before separation current density in this area was much smaller than the density averaged over the whole cell. That is why the measured mean EL intensity increased significantly after separation. These observations are consistent with the model of rather nonuniform current density distribution over the cell area with brighter EL in the low resistance locations. Comparison of our EL images with thermographic images [16] provides additional confirmation to this idea. Enhanced temperature was observed at the periphery of stressed FS cells and attributed to higher Joule heating due to greater current density. We have observed an enhanced EL intensity in this region (see, e.g., Fig.1.7).

The major contributors to the resistance ρ_a are the main diode (ρ_{md}), back contact Schottky diode (ρ_{Sd}) and the CdTe bulk (ρ_{CdTe}) in the quasi-neutral region. The key question is which is dominant under conditions of EL observation and measurement (dark, forward bias)? The main diode resistance exponentially reduces with the forward current increase, while that of the back contact Schottky diode increases and may become the major

contributor. As to the ρ_{CdTe}, all experimental studies and modeling of CdTe/CdS cells show that its contribution is much smaller than the sum of the two others and can be neglected at room temperature. The major contribution of back contact to the area resistivity at forward bias, ρ_{fb}, in the degraded cells is confirmed by numerous studies. In particular, we may refer to Fig. 1.7 above. Then the back contact resistance controls the current density. Thus spatial fluctuation of ρ_{Sd} determines to a great extent the observed EL non-uniformity and its increase with stressing.

The most severe increase in series resistance with stressing which should be attributed to the back contact Schottky diode degradation was observed for the FS cells. It was accompanied by the most dramatic increase in the EL non-uniformity, which indicates a very non-uniform rate of Schottky diode degradation. Important questions arise from these observations. Why do FS cells demonstrate the most nonuniform back contact? Why does this nonuniformity increase with stress significantly faster than for the cells prepared with different deposition techniques and different back contact recipes? What are the mechanisms of the Schottky diode degradation (oxidation of CdTe underneath the metallization, migration of the dopant (Cu) out of the back contact, transformation of the electrically active defects, etc.)? We believe EL measurements in conjunction with other techniques can be a useful additional tool for studies aimed at clarification of these problems.

1.4.2   EL and LBIC measurements on intentionally nonuniform cells

As an example of how EL can be used to clarify the role of Cu in a back contact, CdTe cells with intentionally introduced lateral nonuniformity were fabricated. Doping with copper during application of back contact is a common processing step for CdTe/CdS cell and module fabrication. Along with optimization of doping level (acceptor concentration) in the CdTe bulk, this is aimed at reducing the resistance of back contact. Diffusion of Cu from the top surface of CdTe provides an enhanced acceptor concentration (space charge density) in the vicinity of interface with the metal contact. This in turn makes the Schottky barrier thinner and more transparent for holes via tunneling. The amount of Cu diffused is important for the back contact quality, thus influencing the EL pattern. The latter, in particular, is illustrated by Fig. 1.6 showing the EL images for two cells with ZnTe:Cu/Au back contacts. Deposited Cu diffuses to

both CdTe and ZnTe. The quality of the back contact depends strongly on the Cu/ZnTe ratio [17]. While EL from the cell with higher Cu/ZnTe ratio is rather uniform, the other cell (2.3 times lower ratio) demonstrates a pattern of bright spots on the darker background indicating considerable nonuniformity.

In this study we used a simpler Cu/Au back contact proved previously to provide cell efficiency only slightly below the ZnT:Cu/Au contact, although the stability of the latter was higher. Devices were made with TCO/CdTe/CdS structures processed at First Solar, LLC. Postdeposition treatment and back contact application were conducted at CSM. Material is first etched with a 1% Br:Methanol mixture. After rinsing and drying, a 30 Å Cu layer is evaporated on the CdTe surface. After annealing at 200°C for 7 minutes, excess Cu is etched from the surface. Finally, a 500 Å layer of Au is thermally evaporated in 3.2 mm diameter dots. In order to introduce controlled Cu nonuniformity the standard procedure was modified. Instead of deposition of Cu over the entire CdTe surface, Cu was evaporated in small dots through a mask with holes of ~150 μm in diameter, spaced ~370 μm apart, center-to-center. The result was a Au dot cell with numerous small Cu dots underneath, occupying ~15% of the cell. The process and the geometry of a cell are illustrated in Fig. 1.9 below. This cell was compared to a standard cell processed with Cu deposited over the entire back of the CdTe film.
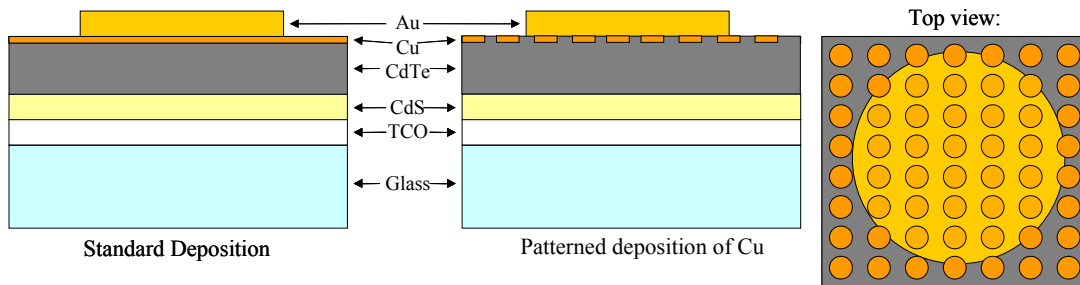
Fig. 1.9. Schematic of patterned deposition to intentionally introduce non-uniformity

It was suggested that areas doped with Cu should have a lower back contact resistance hence greater current density than the undoped areas, thus providing higher EL intensity. This effect is exactly what is seen in the EL images below.

Standard Deposition   Patterned deposition of Cu
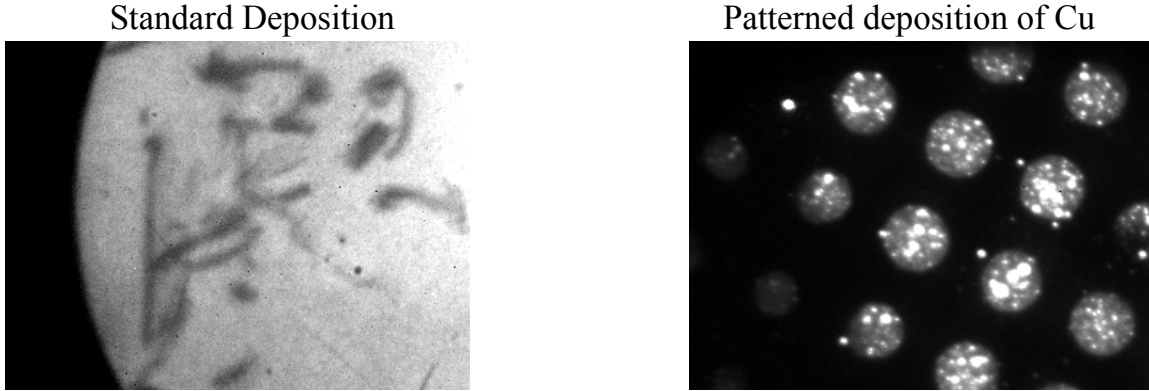
Fig. 1.10 Integrated EL maps of Au/Cu contacted FS CdTe
EL emission for a cell with uniformly deposited Cu (left) and patterned Cu deposition (right) for the same average current density. Dark marks in the left image are caused by scratches from contacting. Dim EL emission was in fact seen in areas without intentional Cu, however it was ~10 times less than in the areas with Cu.

Figure 1.11 shows the effect of the non-uniform doping on dark I-V curves. The resemblance to Fig. 1.8 suggests that the cell with intentionally introduced nonuniformity may be similar to the degraded FS sample. In turn, it strongly supports the idea that the non-uniform degradation of the back contact specific resistance (ρ_{Sd}) provides a significant contribution to nonuniformity in EL distribution. Conversely, studying EL is a convenient (nondestructive) test of the back contact resistance non-uniformity and its evolution under stressing.
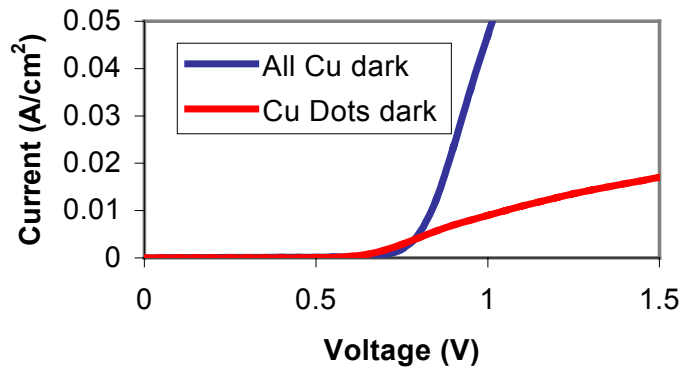
Fig. 1.11.   I-V measurements for standard cell and patterned cell in Fig. 1.10.

After showing that non-uniform back contact specific resistance is an important contributor (perhaps dominant) to EL nonuniformity, we still need to study and evaluate other possible mechanisms using other independent experimental methods.

In collaboration with CSU (Prof. Sites' laboratory) we have obtained and compared EL and LBIC images of exactly the same region of an intentionally nonuniform (Cu-dotted) cells. S. Feldman (CSM) and T. Nagel (CSU) have co-designed and realized a portable stage for cell mounting and contacting that allowed both EL (at CSM) and LBIC (at CSU) mapping. Thus the physical damage to the cell due to re-contacting was minimized. Mapping the entire cell and then lining up large features provides a direct comparison between EL and LBIC data.

Fig. 1.12 shows the EL image for the Cu-dot patterned cell. Figs. 1.13 presents the LBIC images obtained on the same cell at two different excitation wavelengths: 638 nm and 788 nm.
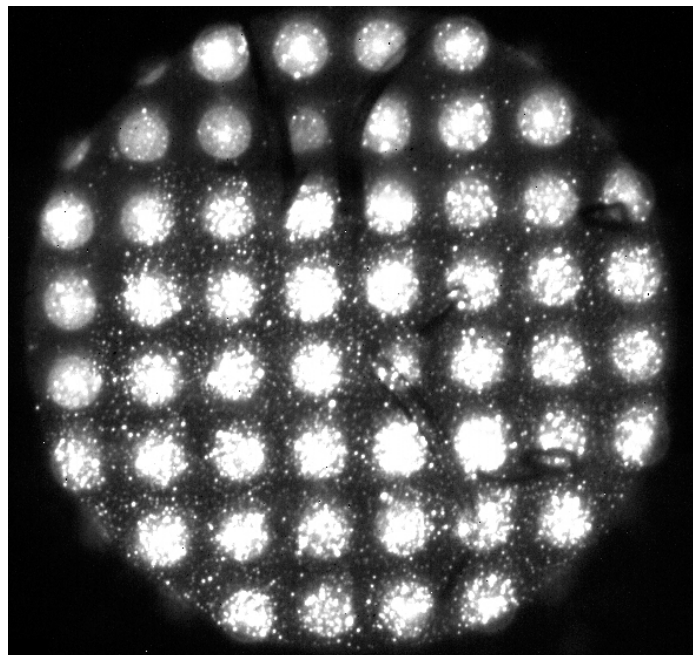
Fig.1.12. EL image of the Cu-dotted cell

Cu Dot LBIC 638 nm laser
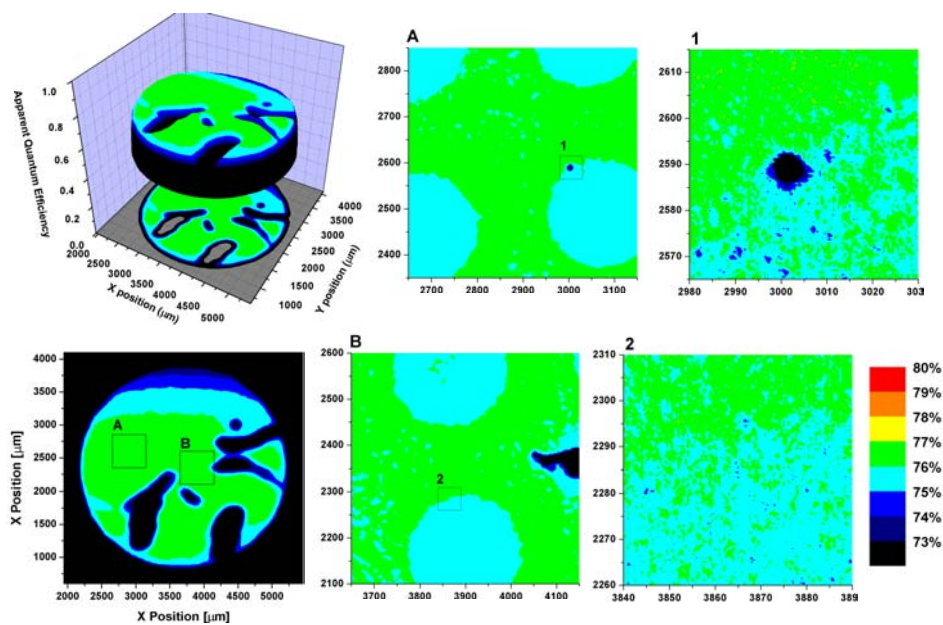
(a)

Cu Dot LBIC 788 nm laser
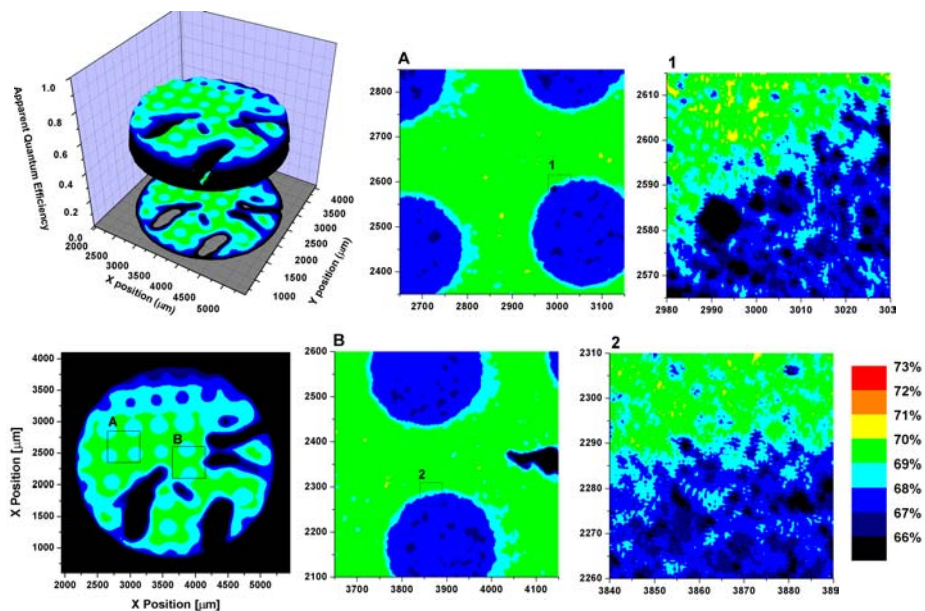
(b)

Fig. 1.13.   LBIC images on the same cell as in Fig. 1.12. (a) λ= 638 nm; (b) λ= 788 nm

LBIC images of the whole cell clearly distinguish between the "Cu" and "no-Cu" areas. Higher magnification images obviously show that the "Cu" areas provide lower photocurrent collection than the "no-Cu" ones. However the differences are rather small: ~1% for λ=638 nm and ~2% for λ=788nm. As compared to this, the contrast in the EL intensity is ~10x between the "Cu" and "no-Cu" areas (Fig.1.12). Thus, if we attribute the EL nonuniformity to a laterally nonuniform back contact resistance, this variation in resistivity does not effect the current collection from these areas. This can be explained by the fact that EL is measured at forward current/voltage so that the back contact Schottky diode resistance dominates, while the photocurrent J_{sc} flows in the reverse direction that makes the back contact resistance negligibly small compared to the main diode. This suggestion is supported by Fig. 1.14 showing the J-V characteristics for cells with different Cu/Au back contact structures.

(a)	(b)	(c)
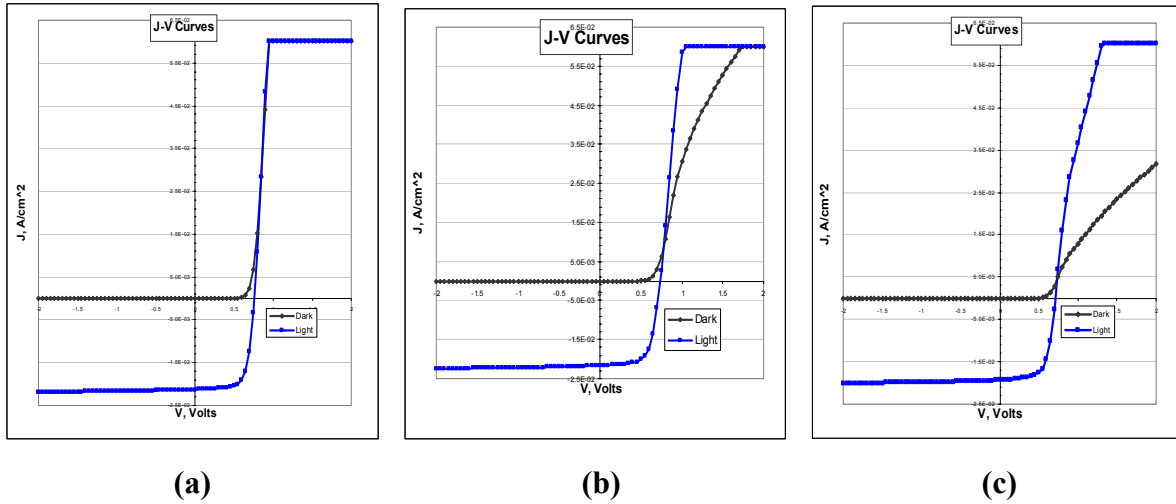
Fig1.14. Light and Dark J-V characteristics
Dark (black) and light (blue) J-V curves for the cells with (a) Cu/Au back contact, (b) with numerous small Cu dots beneath gold,(c) Au back contact, no Cu at all. Horizontal segments of J-V curves at high forward bias are due to the current limit measured by our system.

First, the crossover and rollover are seen for cell (c) without Cu which indicates a developed high resistance back contact Schottky diode. A less pronounced blocking contact is seen in the Cu-dotted cell (b), but rollover is still seen in the dark curve because Cu was deposited only on 15% of the whole cell area. There are no manifestations of a blocking contact for the cell (a) with the Cu deposited on the whole CdTe surface. Slopes of dark curves at

forward bias are significantly lower for (b) and especially (c) than for the cell (a) indicating dominance of blocking contact resistance. Second, the resistance values derived from the slopes of J-V curves at reverse and zero bias for all three cells are high enough to make the ratio ρ_{Sd}/ρ_{md} negligibly small.

If this explanation is accepted, then one must conclude that the nonuniformity in current losses due to nonuniform recombination of photo-generated carriers is not significant. Two possible reasons could be proposed for this. First, if Cu deposited in dots penetrates the region where a majority of photogeneration occurs (active region), then one must suggest that the Cu-related defects are not too effective as recombination centers. Another possible reason could be that Cu does not penetrate into the active region. Cu diffuses very fast in CdTe in the interstitial state, Cu_i^+. But when the Cu_i^+ ions reach the depletion edge, the built-in electric field pushes them out [18]. Thus the major portion of the active layer can be protected from Cu penetration.

So far the conclusion about the rather small nonuniformity in photocurrent collection is valid only for the intentionally nonuniform cells described above. Cells prepared with common procedures, like those presented in Sec.1.3, can behave differently, especially after stressing. Indeed the LBIC images previously reported by CSU demonstrate significant increase in nonuniformity due to stress. However, when trying to explain this effect, we see at least two mechanisms to be discussed. The first one is again the change in the recombination center density. The other is based on the model of "weak diodes" developed by V. Karpov [6]. He has noted that in some locations in a cell with reduced V_{oc} parameter values, photo- current flows in forward direction that is opposite to the total current through the cell. That means that quantum efficiency measured in the region containing the "weak diode" should be lower than in undamaged areas. EL nor LBIC studies are not capable of distinguishing between these two mechanisms.

1.4.3. PL and EL spatial and spectral scans of intentionally nonuniform cells

As mentioned in Sec. 1.2, we recently obtained a new Princeton Instrument Spec-10:100BR Digital CCD Spectroscopy System with monochromator/spectrograph capable of operation in a two-dimensional imaging mode or a one-dimensional imaging spatial mode with spectroscopic data. Features of the order of tens of μm are easily observed with this spectrometer

and provided an ideal test of the instrument. Therefore the intentionally nonuniform cells (INUC) described in Sec. 1.4.2 with the diameter of the Cu dots ~125 μm were chosen for initial studies with this system. Two-dimensional images of the integrated EL from the area containing a few Cu dots were obtained, as well as linear spatial scans of EL and PL through several (usually tree) dots. These linear scans were spectrally resolved. Measurements were conducted with the sample in the temperature range of 300 K to 60 K. The initial measurements were mostly aimed at testing the system and opportunities it provides; hence their results have not yet provided a systematic and complete picture of PL and EL. However, we present here some results indicating that the approach for the comparative EL and PL studies we have chosen is promising and could be fruitful.

The PL and EL spectra are similar and have the same noticeable features (see Fig. 1.15). Both have tiny features in the high-energy range (1.55 eV) provided probably by band-edge transitions. A strong band with a maximum located at 1.36-1.38 eV is probably the same as observed in Cu doped CdTe cells at about 1.40 eV in [19]. Note that our spectra were recorded at T=150 K while those in [19] at T=10 K. This explains some difference in the position of the band. Because our CCD is based on Si sensors, we were able to observe features at lower energies than in [19] (which can also shift peak location). The most prominent were two peaks at ~ 1.33 eV and at ~ 1.25 eV. In some spectra we could see a third peak between the two with smaller amplitude.
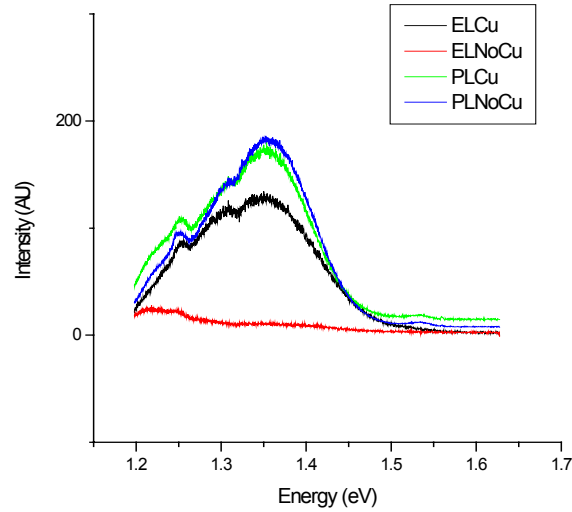
Fig.1.15.   PL and El spectra from "Cu" and "no-Cu" regions

Identification of these three features is not unambiguous. There is a significant discrepancy in literature in attribution of the experimentally observed levels in CdTe as well as in estimates of the energy level for a specific defect. In Ref. [19] a feature at about 1.4 eV is ascribed to a transition of an electron from the conductance band to the Cu_{Cd} state (in Fig. 1.14 it corresponds to the 1.36-1.38 eV feature). In Ref. [7], where cathodoluminescence was studied on CdTe films, a peak at ~1.32 eV observed at T = 77 K is attributed to the same transition. Our peak at ~1.25 eV is closer to the energy of the Cu_{Cd} acceptor level ($E_v + (0.3-0.35)$eV) reported in experimental studies of transport phenomena [20], and DLTS [21]. However, recent theoretical calculations suggested a level of 0.22 eV above the valence band [22]. If our peak of ~1.25 eV is really related to Cu_{Cd}, then a question becomes what are the origins of the two (or three, see Fig. 1.16 and text below it) other peaks?

The recorded spectral El intensity an area without Cu in Fig. 1.15 is very low, which corresponds to the dark area in the two-dimensional image of integrated EL and can be explained by low current density/high back contact resistivity. However, one can see an enhanced intensity (counts) in the low photon energy range (<1.3 eV), which may be related to injection level. With PL, however, we did see variation of the spectrum with the excitation level (see Fig. 1.16).
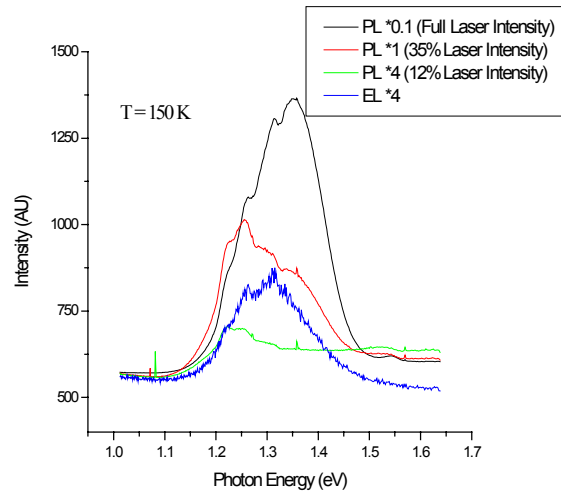
Fig. 1.16. PL intensity at various excitation levels.
Laser intensity was varied by using grey filters. To make all spectra comparable, the measured PL intensity was multiplied by the factor of 0.1 for full Laser intensity of ~20mW/cm^2, and by the factor of 4 for 2mW/cm^2. No multiplication for 7mW/cm^2. For comparison, the EL spectrum (multiplied by the factor of 4) is shown excited by the average current density of 25mA/cm^2.

It is clear that the ratio of the intensity lower energy to higher energy transitions significantly increases as the excitation level (laser power) is reduced. With a tenfold power reduction the PL intensity in the ~1.38 eV peak drops below that in the 1.25 eV region which becomes the most pronounced feature. The spectrum at $7mW/cm^2$ excitation power obviously demonstrates four distinct features in the range of 1.2-1.4 eV. Another effect to be noted is a rapid growth in the integrated PL intensity, I_{PL}, with the laser power: $I_{PL}(20W/cm^2)/I_{PL}(2W/cm^2)\sim100$.

More detailed studies of the influence of excitation level (laser power or current density) on the luminescence intensity and spectrum could provide a better understanding of origin of the observed features and identification of defects responsible for them. On the other hand, variation of excitation level may allow detection and study of some features not observed otherwise.

The last figure in this section presents the spatial scans of EL and PL intensity demonstrating non-uniformity in the intensity distribution both for integrated luminescence and luminescence from a specific wavelength range. Measurements were done at T=150 K. Bumps in EL intensity scans (Fig. (a)) correspond to the "Cu" areas and minima to the "non-Cu" ones. No spatial correlation is seen between EL and PL intensity for the integrated luminescence intensity. Three PL minima in the scan (b) recorded at the photon energy of 1.28 eV are located in the "Cu" areas that demonstrate maximum EL. Thus we see here "anti-correlation" between the PL and EL distribution. It is harder to make definite conclusions about two other traces for photon energies of 1.37 eV and 1.46 eV. Locations of the PL maxima are shifted with respect to those of EL but the phase shift is far from 0 or 180 degrees, therefore it would be too difficult to make conclusions on correlation or anti-correlation. What is doubtless is that the characteristic spatial scale for the major PL nonuniformity is the same as for EL and corresponds to the Cu-dots separation. Since PL is measured at open circuit conditions (no current) the non-uniformity of the back contact resistance to the first approximation should not affect the PL intensity and spectra. That means that PL is sensitive to the presence of Cu so the latter effects the non-radiative recombination. Further studies are underway to obtain more statistically representative results and to make definitive conclusions.
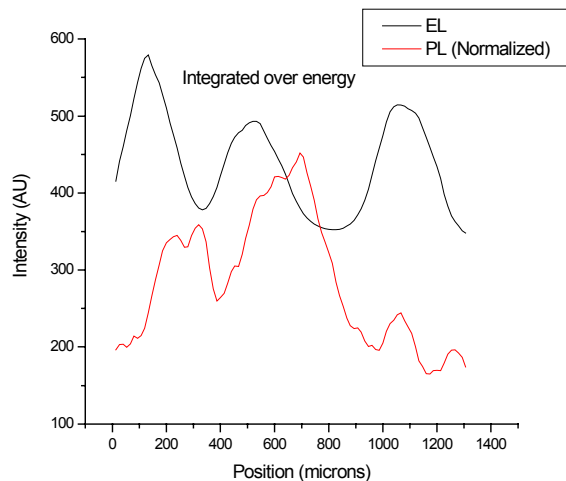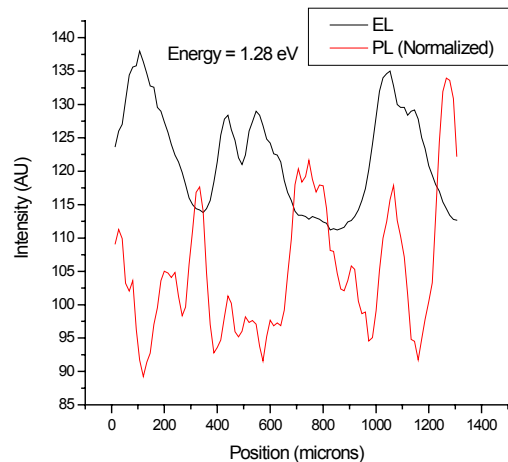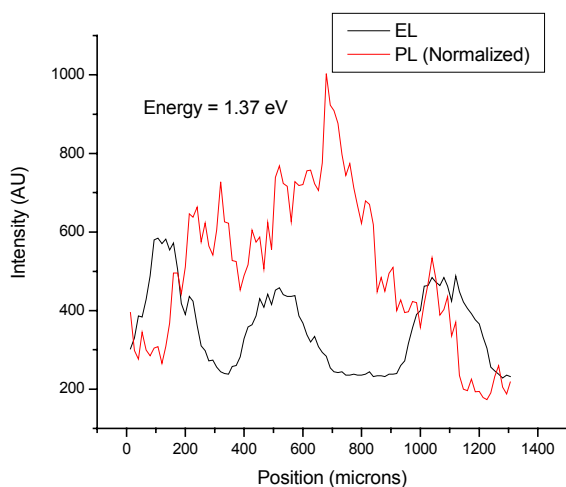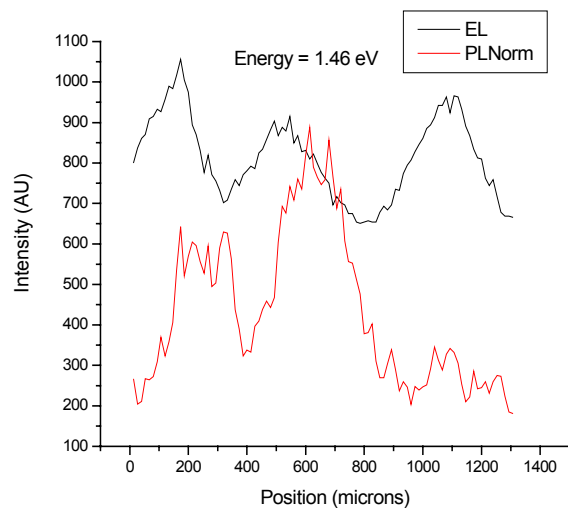
Fig. 1.17. Linear scans of electro- and photoluminescence. (a) integrated luminescence; (b) E_{ph} =1.28 eV; (c) E_{ph} =1.37 eV; (d) E_{ph} =1.46 eV. T=150 K.

2. STUDIES OF DEEP ELECTRONIC STATES

2.1 Introduction.

Deep electronic states are a common concern for the developers and manufacturers of solar cells. First, these states may act as recombination centers, reducing the lifetime of photo-generated carriers, hence photocurrent collection and cell efficiency. This effect competes with the inevitable band-to-band recombination and is especially detrimental for the indirect gap semiconductors like Si, where the lifetime controlled by radiative band-to-band transitions is rather high. Direct gap semiconductors like CdTe are much less sensitive to recombination centers because their band-to-band lifetime is in the range of 10^{-8} s. Therefore the restrictions on the impurity content and structural defects concentration are less severe than for Si. However, in the case of thin film polycrystalline CdTe we are dealing with material containing many structural defects. In addition the fine grain structure of the film (grain size of $\sim 1\mu$m) inevitably introduces a very high concentration of deep electronic states in the gap that could act as recombination centers.

Another aspect of the deep states problem arises when the concentration of traps, N_t, is comparable with or higher than the density of shallow levels that control the majority carrier concentration ("doping level"). In this case traps can significantly contribute to the space charge density in the depletion region, influencing the width of the region where the built-in electric field effectively separates photogenerated electrons and holes, providing higher photocurrent. Recent studies of thin film CdTe cells detected trap densities ($N_t \gtrsim 10^{15} cm^{-3}$) higher than the "doping level" N_{C-V} determined from C-V profiling, [14, 23-26]. Also high trap concentration can lead to significantly overestimation of the doping level [27]. For CdTe the analysis and the estimates of possible errors were presented in [28].

We wish to discuss one more possible effect of the deep states. Deep states of high density may considerably influence free hole concentration (Fermi level position) and its temperature dependence. We have previously discussed the problem with respect to Cu doping effect. SIMS measurements in CdTe:Cu based cells always indicate high Cu concentration, up to 10^{18} cm^{-3}. It is believed that Cu occupies mostly Cd sites, providing an acceptor state. However,

the net "doping level" determined with C-V profiling is usually of the order of $10^{14} cm^{-3}$ at room temperature. Various models were proposed to explain this effect, such as Cu accumulation by grain boundaries while the concentration in the grain bulk is small or strong compensation of Cu acceptor states with the comparable concentration of donors. Here we discuss one more explanation. The real Cu concentration in the grain bulk may be rather high, but free hole concentration is much lower due to only partial ionization of acceptors. Below we present results of modeling based on the assumption that the energy ionization of the level is $E_V + 0.35 eV$ (see e.g., [20, 21])
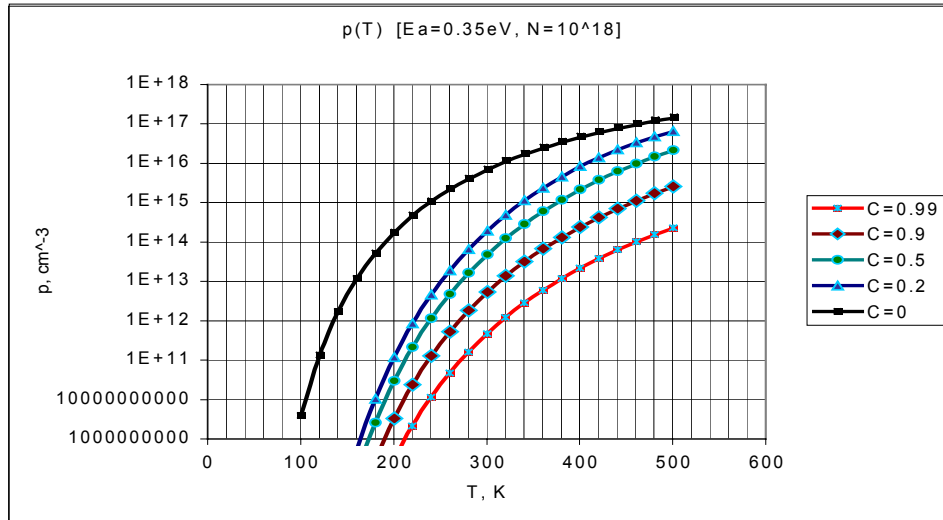
Fig. 2.1. Hole concentration vs. temperature in CdTe for $E_a = 0.35 eV$, $N_A = 10^{18} cm^{-3}$, and varying compensation degree $C = N_D / N_A$

Important conclusions can be made based on the curves in the figure:

- For the assumed energy of the level, hole concentration at room temperature can be much lower than the acceptor density. The difference decreases at elevated temperature and rapidly increases with cooling.

- Compensation decreases ratio p / N_a, especially at lower temperatures.

- Even a slight variation of the compensation degree adjusts the modeled hole concentration to that measured for both suggested acceptor concentrations.

Although the model does not have solid supporting evidence at this time, it deserves to be studied more thoroughly both experimentally and with modeling.

We briefly discussed some aspects of the deep states problem to support the need to continue and further develop studies of deep states in CdTe thin film solar cells. However, our own experience and analysis of other investigations revealed numerous problems we have to solve to be successful. This urged us to review our previous results, revise experimental methods and approaches to the data interpretation, develop new instrumentation, measurement and data analysis procedures. In this section we present results obtained so far.

We begin (Sec. 2.2) with a brief description and discussion of the admittance spectroscopy (AS) method and modifications we have used for studying deep states in CdTe cells. Then we briefly discuss the results of these studies, mostly those that revealed the specific problems to be discussed in Sec. 2.3. The latter is devoted to the analysis of the problems we face when applying widely used AS methods or deep level transient spectroscopy, their technical limitations, and shortcomings of common theory used for the data interpretation. We discuss alternative approaches that can help, at least partially, to overcome the problems revealed by previous studies. In particular, we are focusing on measurements of transient effects, detecting and studying very slow, metastable states. Sec. 2.4 contains description of our recent developments in the technique of measurements aimed at realization of the alternative approaches. Finally, in Sec. 2.5, we present and briefly discuss some of results obtained with a new measuring system.

2.2 Admittance Spectroscopy of Deep States in CdTe Based Cells.

2.2.1 Admittance Spectroscopy Basics

AS is based on the measurement and analysis of frequency dependent admittance/ impedance. Trap recharging (capture/emission of free carriers) caused by application of AC voltage to the diode (cell) leads to the appearance of AC current that has both out-of-phase and in-

phase components providing correspondingly the imaginary and real parts of admittance, Y, and impedance, Z. LCR meters usually display the data in the "parallel, p," and "series, s," modes as $G_p = 1/R_p \equiv \mathrm{Re}(Y)$, $R_s \equiv \mathrm{Re}(Z)$, and $C_p \equiv \mathrm{Im}(Y)/\omega$, $C_s \equiv [\omega \cdot \mathrm{Im}\,Z]^{-1}$. The equivalent electrical circuit of a cell could be more or less complicated, therefore it is important to be cautious when extracting the trap related parts of capacitance, $C_t(\omega)$, and conductance, $G_t(\omega)$, from the raw data provided by LCR meter. Dependence on frequency of C_t and G_t arises from the finite rates of capture/emission processes. Each deep state (trap) has its own characteristic frequency ω_t (inverse characteristic time: $\omega_t = 1/\tau_t$) usually close to the emission rate. For a simple circuit: main diode + single level traps in the depletion region, the frequency dependencies are described by Eqs. (2.1-2.3) and illustrated by the following schematic figures

$$C(\omega) = C_d + \frac{C_t^o}{1+(\omega/\omega_t)^2} \qquad (2.1)$$

$$G(\omega) = G_d + \frac{G_t^o(\omega/\omega_t)^2}{1+(\omega/\omega_t)^2} \qquad (2.2)$$

$$G_t^o = C_t^o \omega_t \qquad (2.3)$$
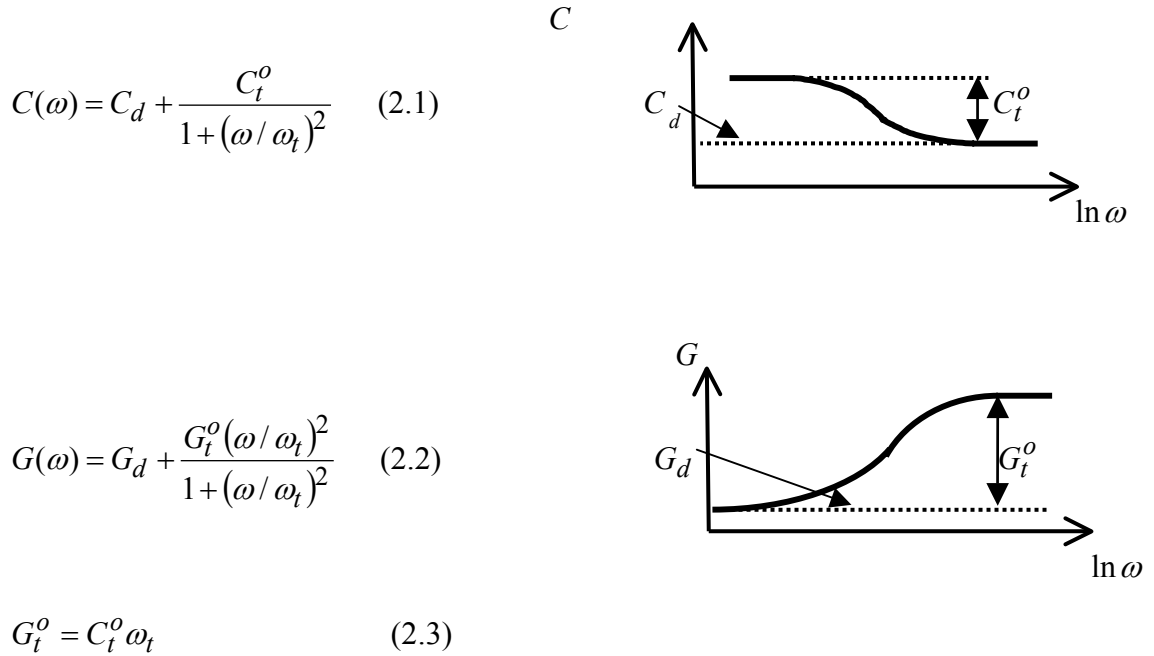
Here C_t^o and G_t^o are the maximum $C_t(\omega)$ and $G_t(\omega)$ values, while C_d and G_d are the parameters characterizing the same diode without traps. These four parameters can be determined by comparison the frequency dependences in the low frequency (LF) and high frequency (HF) limits, respectively at $\omega << \omega_t$ and $\omega >> \omega_t$:

$$C_d = C(\omega_{HF}); \ G_d = G(\omega_{LF}); \ C_t^o = C(\omega_{LF}) - C(\omega_{HF}); \ G_t^o = G(\omega_{HF}) - G(\omega_{LF}) \qquad (2.4)$$

The trap characteristic frequency can be determined from any of the four frequency dependent functions: $-\dfrac{dC}{d\omega} = \varphi_1(\omega); \ \dfrac{dG}{d\omega} = \varphi_2(\omega); \ -\omega \cdot \dfrac{dC}{d\omega} = \varphi_3(\omega); \ G/\omega = \varphi_4(\omega)$. Each has a peak whose position is determined by the trap characteristic frequency:

$$\omega_{peak} = \omega_t / \sqrt{3} \ \text{for} \ \varphi_1 \ \text{and} \ \varphi_2; \ \omega_{peak} = \omega_t \ \text{for} \ \varphi_3 \ \text{and} \ \varphi_4 \quad (2.5).$$

For φ_4 it is so if $G_D \ll G_t$, which is usually the case for our cells.

Which of the functions is more suitable to utilize depends on the properties of the main diode, trap characteristics, conditions of measurements, e.g. bias, light/dark conditions, etc. When the LF or HF limits are not available for the instruments in use, but the peaks in the $\varphi_i(\omega)$ dependencies are within the available frequency range, then the trap related parameters can be determined as $C_t^o = 2\omega_t \cdot \varphi_3(\omega_p)$ and $G_t^o = 2\omega_t \cdot \varphi_4(\omega_p)$ or, by similar analysis of φ_1 and φ_2.

The position of the trap energy level in the bandgap is usually derived from the temperature dependence of the characteristic frequency based on the equation (specified for the hole trap):

$$\omega_t = 2\sigma_t \cdot \langle v_{th} \rangle \cdot N_v \cdot \exp\left(\frac{E_t - E_v}{kT} \right) \qquad (2.6)$$

where $E_t - E_v$ is the trap level energy with respect to the valence band edge, $\langle v_{th} \rangle \propto T^{1/2}$ is the average thermal velocity, $N_v \propto T^{3/2}$ is the effective density of states in the valence band and σ_t is the trap capture cross section. If the Arrhenius plot $\ln(\omega_t / T^{-2})$ vs. $1/T$ provides a linear graph, then the activation energy $E_t - E_v$ is derived from the slope. The intercept of the extrapolated straight line with the $1/T$ axis provides the value of the product $\gamma \cdot \sigma_t$ where

$\gamma = \dfrac{N_v \cdot \langle v_{th} \rangle}{T^2} = \dfrac{16\pi \cdot k^2 \cdot m^*}{h^3} \approx 3 \cdot 10^{21} \cdot \dfrac{m^*}{m_o} (cm^2 \cdot K^2 \cdot s)^{-1}$. Thus the only parameter we need to know is the effective mass. There is some uncertainty in the effective mass value we must use in calculations because of the complicated valence band structure in CdTe (degenerate heavy and

light hole bands) as well as the spread in published values for both. However, if we use $m^*/m_o \approx 0.8$, the possible error should not exceed a few tens %. Other factors can dominate the error, e.g., nonlinear graph, errors in the extrapolation, etc. Uncertainty in the estimate of σ_t within one order of magnitude could be considered acceptable.

To estimate the trap concentration from AS data, the simple theory for a single trap level, and uniform distribution of "doping level" N and trap concentration N_t, provides an equation:

$$\frac{C_t^o}{C_d} = \frac{N_t}{N}\frac{1-x_t/x_d}{1+(N_t/N)\cdot(x_t/x_d)} \tag{2.7}$$

where x_d is the depletion width and x_t is the "crossing point", the distance from the interface where the deep level crosses the Fermi level, $E_t(x_t) = E_F$. For a small x_t/x_d ratio, e.g. at forward bias, $C_t^o/C_d \approx N_t/N$. Thus, if one observes $C_t^o/C_d \geq 1$, that means that the trap density is higher than the "doping level". Indeed, sometimes we have observed a two- to threefold decrease in capacitance value with increasing frequency. It is hard to make more definite quantitative estimates because of the assumptions of the concentrations uniformity. In the case of small trap concentration ($N_t << N$), Eq. 2.7 takes a simpler form:

$$\frac{C_t^o}{C_d} = \frac{N_t}{N}\left(1-\frac{x_t}{x_d}\right) = \frac{N_t}{N}\left(\frac{U_t}{U}\right)^{1/2} \tag{2.7a}$$

where $U = V_{b-i} + V_{bias}$ is the total band bending and $U_t \equiv (E_t - E_F)/e$.

2.2.2 Modifications of Admittance Spectroscopy

We have also used two modifications of AS for studying trap density of states in CdTe cells. As formulated, both methods can be applied not only to detecting and studying single levels or isolated trap levels, but also to study and quantitatively estimate continuous distribution of trap levels over energy.

The first modification developed by Walter et al. [29] proposes the following equation for deriving the trap density of states, D_t, (DOS), from the capacitance frequency dependence:

$$D_t(E_\omega) = -A(U, E_F, x_d) \cdot \frac{dC}{d\omega} \cdot \frac{\omega}{kT} \qquad (2.8)$$

Here A is a coefficient that depends on the total band bending, U, Fermi level position in the quasi-neutral region, E_F, and depletion width, x_d. The energy E_ω is calculated as

$$E_\omega = kT \cdot \ln(2\nu_o / \omega) \qquad (2.9)$$

where $\nu_o = \sigma_t \cdot \langle v_{th} \rangle \cdot N_v$ is the "attempt-to-escape" frequency.

For CdTe at T = 300 K, $\nu_o(s^{-1}) \approx 10^{26} \cdot \sigma_t(cm^2)$, e.g., $\nu_o \approx 10^{12} s^{-1}$ for $\sigma_t = 10^{-14} cm^2$. E_ω is the demarcation energy between trap states that can recharge under the AC voltage of frequency ω and those that are not able to follow oscillations of testing voltage. With increasing testing frequency E_ω shifts toward the valence band.

In the case of small trap concentration ($N_t \ll N$) and uniform doping level

$$A(U, E_F, x_d) = \left(\frac{N}{2e\varepsilon\varepsilon_o}\right)^{1/2} \frac{U}{U_\omega^{1/2}} \qquad (2.10)$$

where $U_\omega = \dfrac{E_\omega - E_F}{e}$.

The DOS function can be also derived from the conductance dependence on frequency:

$$D_t(E_\omega) = -A(U, E_F, x_d) \cdot \frac{d}{d\omega}\left(\frac{G}{\omega^2}\right) \cdot \frac{\omega^2}{kT} \qquad (2.11)$$

Thus, this method, contrary to the standard AS, can provide information not only on single trap levels that manifest themselves as peaks in DOS function, but also on trap level bands and continuous distribution of deep states in the bandgap. It should be mentioned that single levels and bands could not be distinguished if the width of the latter does not exceed (2-3) kT.

Since $E_\omega \propto T$, measurements at different temperatures widen the range of energies for which DOS can be determined. Integrating the measured DOS function over energy provides the concentration of various traps. Note that only traps located in the vicinity of the crossing point contribute to the measured capacitance. With increasing trap energy, the crossing point moves toward the interface. Thus, $D_t(E_\omega)$ is actually determined at different locations. If the DOS function is spatially uniform, this method can provide exact and unambiguous information.

The second modification, drive level capacitance profiling (DLCP) method presented in [30], is also aimed at determination of the trap DOS function. The method is based on measuring capacitance at a fixed frequency and makes use of the dependence of the measured capacitance on the amplitude of the AC testing voltage. As the amplitude δV ("driving level") increases we obtain higher order on δV corrections to the capacitance. At relatively small δV, $C \approx C_o + C_1 \delta V$ and the density of trap states can be determined as

$$N_t'(E_\omega) = -C^3/(2e\varepsilon\varepsilon_o A^2 \cdot C_1) \tag{2.12}$$

Here E_ω has the same meaning as before and is determined by Eq. 2.9. $N_t'(E_\omega)$ is the concentration of traps of energy below E_ω at the distance $x_{t\omega}$ from the interface where the Fermi level crosses the level E_ω. Varying the applied DC bias voltage V_{bias} can change the crossing point position. By measuring $C(\delta V)$ at different biases we can obtain information on the spatial distribution of $N_t'(E_\omega)$. Since E_ω depends on testing frequency and temperature, measurements of the same kind at varying frequency and temperature provides broader and more detailed information on the DOS function and its spatial variation. Again we must note that due to variation of E_ω hence $x_{t\omega}$ with frequency, the shape of the DOS dependence on energy could be determined correctly only if the DOS does not depend on distance. If it does depend, we face also the problem of uncertainty in location at which $N_t'(E_\omega)$ is measured. Measurements at varying bias, due to moving crossing point $x_{t\omega}$ can provide at most the trends in spatial dependence of DOS.

2.2.3 Major Results of the Deep States Studies in CdTe Cells

Admittance spectroscopy measurements at CSM were performed on cells fabricated at various facilities (FS, NREL, UT, CSM) with various processing techniques. Specifically, the effects of back contact, CdCl$_2$ treatment and etching of CdTe surface were studied. In nearly all cells a high trap concentration was found with non-uniform spatial distribution.

Fig. 2.2 shows typical frequency dependencies of capacitance and conductance measured on the FS/CSM cells with Cu/Au back contact. Measurements were done using two LCR meters; one for the frequency range of 20 Hz to 1 MHz and the other for 75 kHz to 30 MHz. Switching from one to the other sometimes introduced a small shift in displayed capacitance like that seen in the left figure. Compensating the shift provides a continuous graph with smooth variation of the slope. The shift is insignificant in the $G(f)$ dependence.
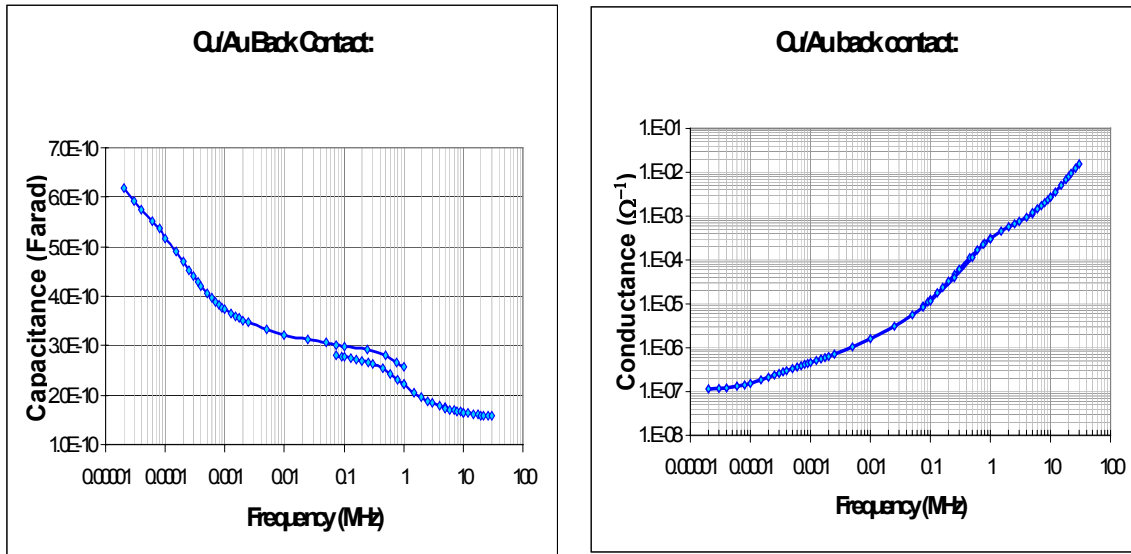
Fig. 2.2. Capacitance and conductance of a FS/CSM cell with the Cu/Au back contact measured at room temperature

The shape of both dependencies correlate with the trap concept and equations presented in Sec. 2.2.1. The capacitance value gradually decreases while the frequency changes several orders of magnitude. This suggests the presence of several types of traps or a continuous

42

distribution of levels and characteristic times. The two-fold decrease in C between 20 Hz and 100 KHz means that the total density of traps with characteristic times in the range of $\sim 10 ms$ to $\sim 1.5 \mu s$, exceeds $N_{C-V} \approx 3 \cdot 10^{14} cm^{-3}$ for this cell at zero bias. Reduction of capacitance without saturation at higher frequencies indicates the presence of faster traps. The $C(f)$ dependence does not manifest any tendency to saturation at low frequency indicating the presence of slower traps ($\tau > 8 ms$).

To examine the slower traps we studied capacitance changes after switching the applied bias, which revealed long-term transients, with relaxation times varying from seconds to minutes to hours. This may be at least partially attributed to changes in the space charge density caused by slow reoccupation of traps by carriers. Based on the theory of transients [27] we estimated the concentration of slow traps responsible for the observed effects was $N_t^{slow} \gtrsim 10^{15} cm^{-3}$.

The (dG/df) vs. f plot in Fig.2.3 demonstrates two peaks that could be attributed to single levels or relatively narrow trap bands of enhanced trap DOS. The characteristic times derived from the peak frequencies are ~1.6 ms and ~0.35 µs. The trap concentrations estimated from the peak magnitudes are comparable to the "doping level" for both peaks.
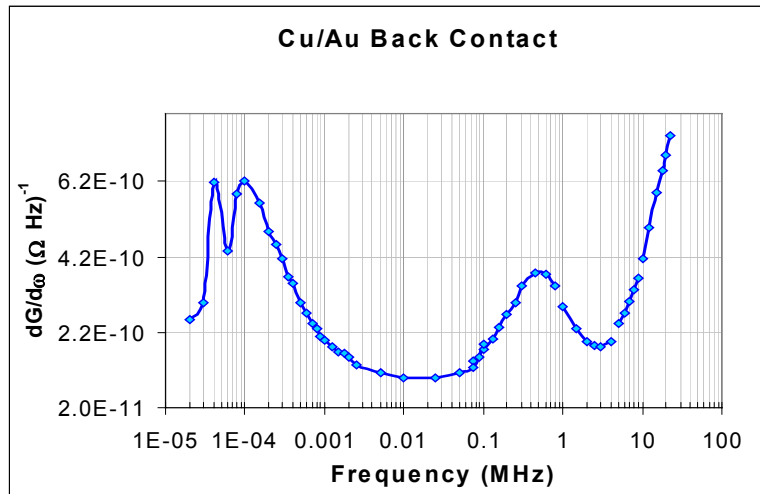
Fig. 2.3. $(dG/df) - f$ plot has two peaks with characteristic times of 1.6 ms and 0.35 µs

Application of the Walter/Herberholz method [29] described in Sec. 2.2.2 showed the presence of the narrow band centered at the energy $E_\omega \approx 035\text{-}0.4$ eV (depending on temperature). The maximum DOS value was $\sim 2 \cdot 10^{16} eV^{-1} cm^{-3}$. We estimated the total concentration of traps in the band as $\sim 1.5 \cdot 10^{15} cm^{-3}$.

Comparison of the results of AS for Cu/Au and Au-contacted cells demonstrates significant effects of Cu dopant. In particular, the high frequency peak ($\Delta E = (0.37 \pm 0.03) eV$) that is well pronounced in Cu-doped cells disappears in the undoped cells. Instead, a small peak at 100 kHz is seen. The decrease in magnitude and some shift in peak position was observed for the low-frequency peak ($\sim$ 100 Hz). Significant differences were noted in transients. Changes caused by stressing are also more significant for cells doped with Cu.

Effect of postdeposition treatment, specifically CdCl$_2$ treatment and etching of CdTe surface, on deep states in CdTe bandgap was studied by using a standard AS and DLCP (Sec. 2.2.2). The FS/CSM cells were studied. Postdeposition treatments and ZnTe:Cu/Au back contact were applied at CSM. Averaged characteristics of differently treated cells are presented in Table 1. Results of AS measurements for typical cell of each type are shown in Fig. 2.4.

Table 2.1. Characteristics of cells with different postdeposition procedures

Cell type	CdCl$_2$ treated	Etch	Eff., %	N_{cv} *) 10^{14}cm^{-3}		Density of traps (10^{14}cm^{-3}) for $E_t<E_\omega$**)					
					x, μm	~2.3		~1		~0.15	
					E_ω***) eV	0.6	0.4	0.6	0.4	0.6	0.4
A	Yes	Yes	10.8	2.3		20	10	25	7	35	9
B	Yes	No	10.5	3.1		25	10	20	8	20	8
C	No	Yes	8.6	1.9		30	8	20	5	25	5
D	No	No	6.2	0.75		10	6	7	3	8	3

*) Doping level at the depth x=1.5μm (from C-V profile at f=100 KHz)

**) Obtained with drive level capacitance profiling (DLCP)

***) Approximate values

The table shows that a significant trap density belongs to the energy range between 0.4 and 0.6 eV; the deeper trap concentration is high at all depths. For all types of cells the estimated trap density is greater than the "C-V doping level". Cells A and B with the highest efficiency both have high trap concentration, while the least efficient cells D (without $CdCl_2$ and etch) have a much smaller trap concentration.

(a)   **(b)**
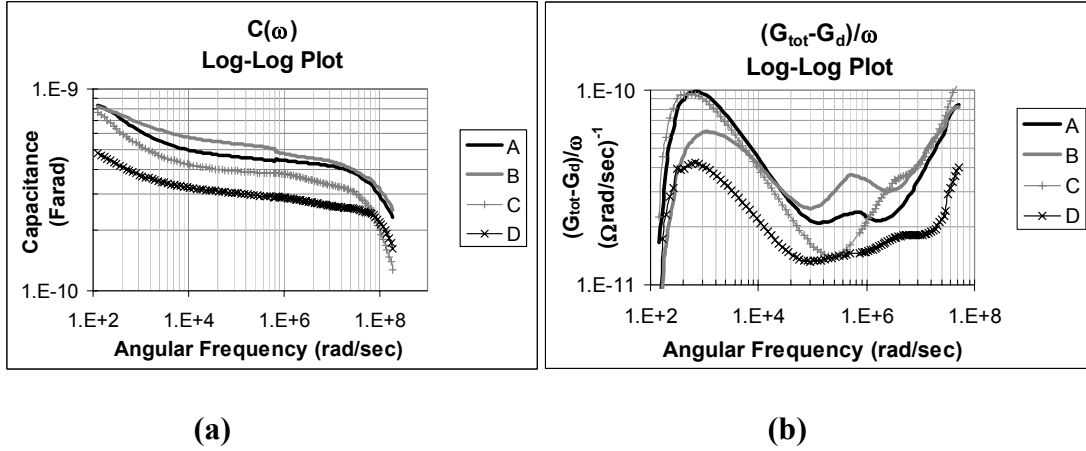
Fig. 2.4.   Results of AS measurements on cells with different postdeposition treatments (see A, B, C, D in Table 2.1)

The results of AS measurements confirm the DLCP results. A significant (about two times) decrease in capacitance (Fig. 2.4.a) means that the total trap concentration in the characteristic time range from 10 ms to 1 μs exceeds the doping level. Peaks in Fig. 2.4.b reveal the existence of several distinct trapping levels or bands with widely varying characteristic frequencies (ω_{peak} = ω_t). Assuming the "attempt-to-escape" frequency ν_o value of $10^{12} s^{-1}$ the trap energy was estimated: for the lower frequency peaks (ω_{peak}~$5x10^2 s^{-1}$) E_t-E_v ~ 0.6eV; for the higher frequency peaks (ω_{peak}~$10^6 s^{-1}$), E_t-E_v ~ 0.4eV. The $CdCl_2$ treatment (cells A and B) increases concentration of states in both bands. For cells C and D (without $CdCl_2$) the peaks at ω_{peak}~$8x10^5 s^{-1}$ are not clearly visible. Instead, peaks appear close to $2x10^6 s^{-1}$. The influence of etching on the conductance spectra is well seen for these two samples.

Differences in trap concentrations and depth profiles were also revealed by DLCP measurements on traps prepared with different CdTe deposition techniques (FS, NREL, UT). For all cells, trap density was minimal in the vicinity of the depletion edge and increased toward the

45

interface and back contact. The highest trap density $1 \cdot 10^{16} cm^{-3}$ was found in the UT cell at reverse bias. The FS cell maximum density was around $1 \cdot 10^{15} cm^{-3}$. For the NREL cell it was in the range of $(4-6) \cdot 10^{15} cm^{-3}$.

2.2.4. Conclusions

The standard admittance spectroscopy and its modifications (Walter et al. [29] and DLCP [30]) applied to studies of thin film CdTe cells provided mutually complementary and non-contradictory information on deep electronic states in CdTe. The main results are:

- In all cells manufactured at different facilities, a high trap concentration was found, sometimes several times greater than the "C-V doping level".
- At least two narrow bands of deep states were detected in the energy range of $0.33-0.4eV$ and $0.57-0.63eV$. There was evidence of a significant amount of deeper/slower traps ($\tau > 10ms$) and probably much slower (~minutes, even hours) traps that are not available for detection with our LCR meters.
- Concentration of traps and their spatial distribution depend on CdTe deposition technique and postdeposition treatment. Significant changes were caused by doping with Cu and stressing.
- No evidence of detrimental effect on cell performance due to enhanced trap concentration was found for the traps detected in these studies ($\tau < 10ms$, $E_t - E_V \lesssim 0.6eV$).

2.3. Some Problems and Possible Approaches to Their Solution

In this section we will formulate and discuss some of the problems related to studies of deep states in our cells.

2.3.1. Effect of High Trap Concentration

The analysis of results of AS and DLTS measurements usually is based on equations valid for small trap concentration: $N_t << N$. As shown in the previous section, CdTe thin film cells have rather high trap concentration. In particular, both narrow bands detected by AS contain

density of states exceeding the "C-V doping level". To illustrate complications caused by high trap concentrations, let us consider a simple model of a single trap level while $N(x) = const.$ and $N_t(x) = const.$ For $N_t \ll N$, the N_t value can be determined from the $C(\omega)$ dependence, if N (hence E_F) and the trap level E_t are already known, by using an equation from Sec. 2.2.1:

$$\frac{C_t^o}{C_d} = \frac{N_t}{N}\left(\frac{U_t}{U}\right)^{1/2} \tag{2.7a}$$

The equation for an arbitrary trap concentration, Eq. 2.7, can be presented in a similar form

$$\frac{C_t^o}{C_d} = F(t,b)\cdot\frac{N_t}{N}\left(\frac{U_t}{U}\right)^{1.2} \tag{2.13}$$

with the correction factor

$$F(b,t) = \sqrt{\frac{1+t(1-b)}{b}} \tag{2.14}$$

where $b \equiv U_t/U$ and $t \equiv N_t/N$.
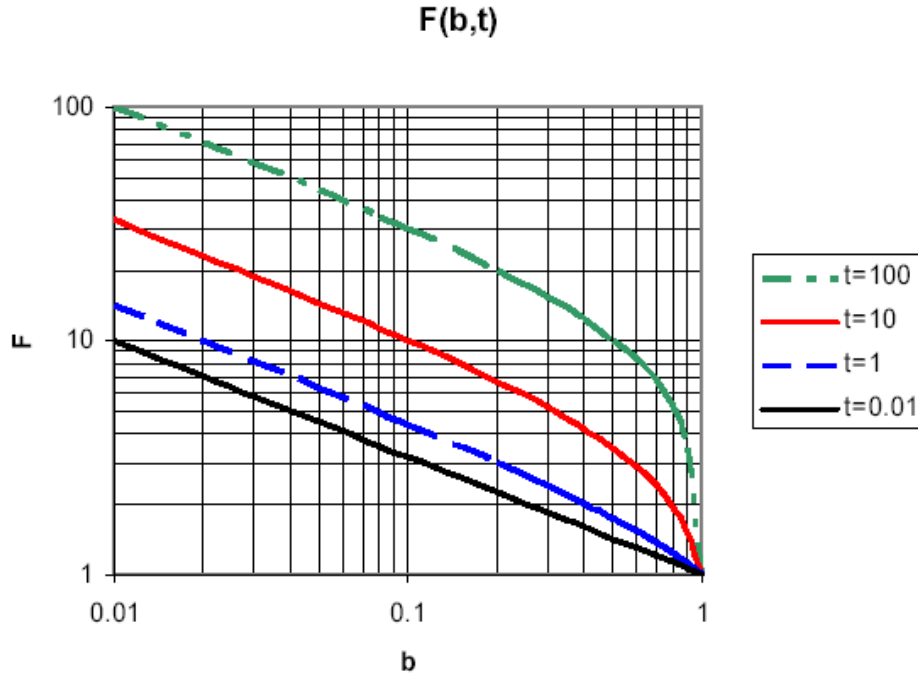
Fig. 2.5. Correction factor $F(b,t)$ in Eq. 2.13

It is seen from the figure that commonly used equation (2.7a) can lead to underestimation of trap concentration, especially significant if the Fermi level is located close to the trap level (small b). The error increases with the N_t / N ratio growth. It should be noted that the Eqs. 2.8 and 2.10 used for the determination of trap density of states when applying modified AS, also should be corrected in a similar way for a high trap concentration.

C-V Profiling in the presence of high trap concentration

We also face another problem when using common theory for estimating trap density from AS measurements. Equations 2.7 and 2.10, corrected or not, allow us to estimate not the trap concentration itself but the ratio N_t / N. Thus to estimate trap concentration or DOS function we need to first determine the "doping level" which is usually derived from C-V measurements. But in the case of high trap concentration the common C-V data treatment procedure can provide incorrect N profiles with an overestimated doping level.

C-V profiling is usually performed with the testing signal frequency as high as possible to exclude the trapped charge oscillations contribution in the measured capacitance. It can be done if the testing frequency is higher than the characteristic frequency of all traps so that the trapped charge cannot follow the voltage oscillations. If this condition is satisfied, measured capacitance is determined by depletion width. Specific capacitance (per unit area of a cell) is

$$C = \frac{\varepsilon \varepsilon_o}{x_d} \tag{2.15}$$

The common approach to the C-V profiling supposes that a change in space charge in the depletion region δQ due to small change in bias δU comes only from the shift of the depletion edge δx_d, hence

$$\frac{dC}{dU} = \frac{dC}{dx_d} \frac{dx_d}{dU} = -\frac{\varepsilon \varepsilon_o}{x_d^2} \frac{dx_d}{dU} \tag{2.16}$$

The space charge density at the depletion edge is $\rho(x_d) = -eN(x_d)$, therefore the change in voltage across the depletion region is

$$\delta U = -\delta\left\{\frac{1}{\varepsilon\varepsilon_o}\int\limits_o^{x_d} x\rho(x)dx\right\} = \frac{e}{\varepsilon\varepsilon_o}N(x_d)x_d\delta x_d$$

and

$$\frac{dx_d}{dU} = \frac{\varepsilon\varepsilon_o}{e\cdot N(x_d)\cdot x_d} \tag{2.17}$$

Eventually, the well known equation to derive the doping profile from C-V measurements is

$$N(x_d) = -\frac{C^3}{e\varepsilon\varepsilon_o}\left(\frac{dC}{dU}\right)^{-1} = \frac{2}{e\varepsilon\varepsilon_o}\left(\frac{dC^{-2}}{dU}\right)^{-1} \tag{2.18}$$

However, Eq. 2.17 is approximately correct only for low trap concentration . The mechanism of the trap effect on the C-V profile is as follows. Small change in the DC bias applied to a cell not only shifts the depletion edge, but equally shifts the crossing points of all trap levels, $\delta x_{ti} = \delta x_d$. If the trap is not too slow and is able to follow the bias changes, this leads to changes in trapped electrical charge. As was pointed by Kimmerling [31] the total time of C-V profiling, as well as the time spent for applying the bias increment and measurements at a new bias, can be much longer than the characteristic time of a trap. In other words, the characteristic time of the bias change, θ, can be (and usually is) much longer than $\tau_t = \omega_t^{-1}$ and ω^{-1}. This means that, while the trapped charge does not oscillate, it follows the changes in DC bias. The effect under discussion has been confirmed by numerous observations of the hysteresis loops in C-V profiles, and correspondingly in $N(x)$ profiles, usually more significant in the latter.

Changes in space charge density within the depletion width influence the dx_d / dU value as illustrated by Eq. 2.19 derived for the multi-level model:

$$\frac{\delta x_d}{\delta U} = \frac{\varepsilon\varepsilon_o}{e}\left\{x_d N(x_d) + \sum_i x_{ti}N_{ti}(x_{ti})\right\}^{-1} \tag{2.19}$$

where summarizing is conducted over all traps with $\tau_t < \theta$ that are fast enough to follow changes in bias. By replacing Eq. 2.17 with 2.19 we obtain the equation for the "apparent" doping level, N', derived from C-V measurements with the common procedure:

$$N'(x_d) = \frac{2}{e\varepsilon\varepsilon_o}\left(\frac{dC^{-2}}{dU}\right)^{-1} = N(x_d)\left\{1 + \sum_i \frac{x_{ti}}{x_d}\frac{N_{ti}(x_{ti})}{N}\right\} \qquad (2.20)$$

To evaluate possible effect of traps on the "C-V doping profile" we have calculated the apparent doping level for a two-trap-level model with trap energy $E_{t1} = 0.4eV$ and $E_{t2} = 0.6eV$, close to those detected in CdTe using AS (see Sec. 2.2.3). The characteristic times determined for these two traps, $\tau_1 \sim 10^{-6}s$ and $\tau_2 \sim 10^{-3}s$, are shorter than the "delay time" provided by our LCR meters, that is the trapped charge follows DC bias changes. The model was simplified by the assumption that the real doping level and trap concentrations are spatially uniform. The results are shown in Fig. 2.6 for the real doping level varying in the range $10^{13}cm^{-3} \leq N \leq 3\cdot10^{14}cm^{-3}$, and two sets of trap concentrations, consistent with the concentrations estimated in Sec. 2.23: (1) $N_{t1} = 3\cdot10^{14}cm^{-3}$, $N_{t2} = 1\cdot10^{15}cm^{-3}$ and (2) $N_{t1} = 1\cdot10^{15}cm^{-3}$, $N_{t2} = 3\cdot10^{15}cm^{-3}$.
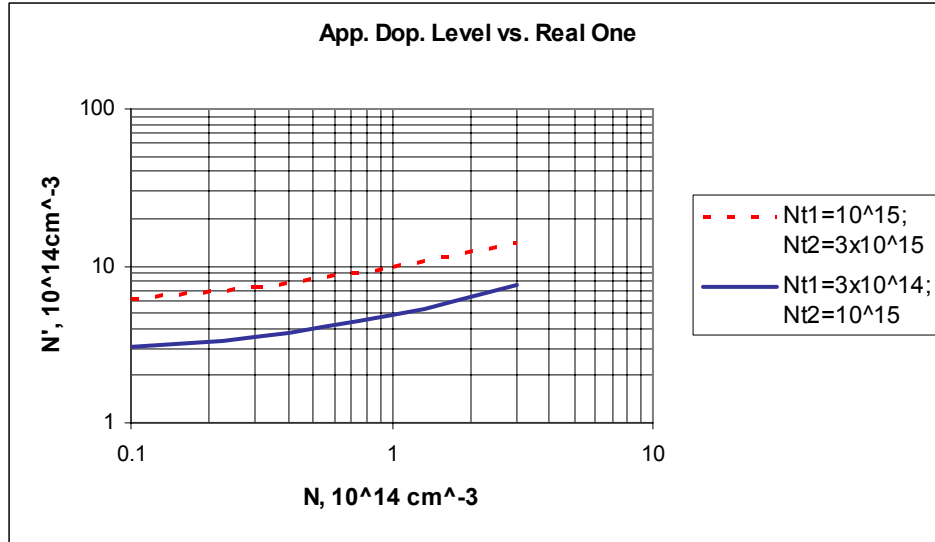
Fig. 2.6. Apparent doping level versus the real one for the two-trap-level model.

The main features of the apparent doping level, N', seen from the figure are:
- The apparent doping level derived from C-V profiling could be significantly higher than the real one for high trap concentration

- N' varies much less than the real doping level N. In our calculations a 30x increase in N is accompanied with only a two- to threefold increase in N'.

- The apparent doping level, calculated for trap density not exceeding the values determined experimentally, is in the range of $3 \cdot 10^{14} - 1 \cdot 10^{15} cm^{-3}$, which is close to what is thought to be the carrier concentration/doping level in thin film CdTe cells. However, we can say nothing certain about the real doping level/free hole concentration based only on C-V measurements.

To cope with the problems discussed above we are moving in two directions:

1. Experimentally obtaining more detailed and reliable information on trap energy level/bands, characteristic times, estimated concentration (or DOS function). To do this we have developed a new system (see Sec. 2.5) and significantly broadened conditions of measurements, such as temperature range, time of monitoring, bias, light intensity and spectrum, etc. AS, C-V profiling and J-V measurements will be accompanied by measurements of transients caused by bias switch, illumination and rapid change in temperature, in the time range from seconds to hours and days.

2. Modeling with the AMPS and SCAPS programs of cell characteristics, including J-V, C-V, C(f), and transients. The greater the information we get from experiment and the greater the number of characteristics we model, the more reliable the estimates we can make of the trap properties.

2.3.2 Technical Limitations on the Characteristic Time of Traps Available for Detection and Studies.

The LCR meters in use limit the frequency range of admittance spectroscopy. In particular, our LCR meters nominally provide measurements in the range of 20Hz to 30MHz, but in reality the range is narrower due to the impact of parasitic effects and noises in the vicinity of upper and lower frequency limits. Another limitation on high frequency range comes from the cell series resistance, which in combination with the cell capacitance provides features in the admittance-frequency dependence similar to those due to traps. [41]. For a well developed back

contact Schottky diode this feature's frequency is temperature-dependent with an activation energy in the range ~hundreds meV.

Thus the AS capabilities to detect and study deep traps are confined to traps with characteristic times in the range of $\tau \sim 10^{-2}$ to $\sim 10^{-6} s$. The major problem is to extend the higher τ limit up to seconds, minutes and hours because there is solid evidence of a significant amount of very slow traps in our cells. The progress in this direction is strongly limited by electronic devices capabilities and principal difficulties of electrical measurements at very low frequencies. For example, accurate measurement of admittance at a single frequency such as 0.01 Hz will take at least tens of minutes, and measurements of frequency dependence in this range – many hours. More feasible solution of the problem is to use the temperature dependence of the trap characteristic time and bring τ into the range available for LCR meter. Indeed for deep levels characteristic time is thermally activated and exponentially depends on temperature. To demonstrate the rate of characteristic time change with temperature the ratio $\tau(T)/\tau(300K)$ was calculated based on the equation $\tau(T) \propto T^{-2} \cdot \exp(E_t / kT)$. The results presented in Table 2.2 show that if the characteristic time is too short at room temperature for a deep level with $E_t = 0.3eV$, it could be increased by ~100 times with cooling to T=220K and much more by further cooling. Conversely, very long $\tau(300K)$ for deeper levels like $E_t = 0.8eV$ can be made ~100 times faster at T=350K (We should be cautious with further temperature increase because of possible irreversible changes of a cell we observed in some experiments).

Another approach to study slow traps, especially very slow ones, is to study and analyze admittance transients with characteristic times in the range of seconds, minutes, hours, days. The most unambiguous information on trap characteristic time and density can be derived from measurements and analysis of capacitance transients. Traps with the characteristic time in the range 10 ms $\lesssim \tau \lesssim$ 10s at room temperature, not detectable by AS and not suitable for the transient studies, could be brought to the desired range by cooling. Since traps of this kind demonstrate a high activation energy we do not need much cooling (see the Table 2.2). Thus, combining AS and transient measurements with temperature variation allows the trap detection and studies in the whole reasonable range of characteristic times.

Table 2.2. Dependence of the characteristic time on temperature: $\tau(T)/\tau(300K)$

T, K	$\tau(T)/\tau(300K)$			
	$E_t = 0.3eV$	$E_t = 0.4eV$	$E_t = 0.6eV$	$E_t = 0.8eV$
350	0.14	0.08	0.027	$8.8\text{x}10^{-3}$
300	1.0	1.0	1.0	1.00
260	7.7	14	50	$1.6\text{x}10^2$
220	$1.3\text{x}10^2$	$5.3\text{x}10^2$	$9.1\text{x}10^3$	$1.5\text{x}10^5$
185	$3.6\text{x}10^3$	$4\text{x}10^4$	$5.0\text{x}10^6$	----
160	$9.1\text{x}10^4$	$2.7\text{x}10^6$	----	----
140	$2.7\text{x}10^6$	----	----	----

2.3.3 Capture cross section. Very Slow Traps.

Analysis of $\omega_t(T)$ data based on Eq. 2.6 and the Arrhenius plot $\ln(\omega_t/T^{-2})$ vs. $1/T$ is

aimed at determination of the trap level distance from the band edge, E_t, and the capture cross

section value, σ_t. The treatment of the data is based on the assumption that the capture cross

section is temperature independent, which sometimes is not true. Even if the Arrhenius plot

provides a straight line graph, the activation energy derived from the slope is not necessarily

equal to E_t. Capture cross section can depend on temperature exponentially

$$\sigma(T) = \sigma_\infty \cdot \exp\left(-\frac{E_\sigma}{kT}\right) \tag{2.21}$$

In this case the activation energy is the sum of two energies ($E_a = E_t + E_\sigma$) and is used only as

a "signature" of a specific trap but does not provide an estimate of the trap level position. At the

same time, the common procedure to derive σ_t from the y-intercept actually estimates the value

of $\sigma_\infty \equiv \sigma(T \to \infty)$, not the real cross section at finite temperature. An approach to determine

$\sigma(T)$ and separate E_σ and E_t from DLTS measurements by varying the filling pulse time is

presented in [27]. For example, application of this approach to InGaAsN alloys [35] suggested

that σ (T) follows Eq. 2.21 with the capture rate activation energy $E_\sigma \approx 0.4eV$. The real capture cross section turned out orders of magnitude higher than that determined from the y-intercept. This kind of $\sigma(T)$ dependence is usually explained based on the model of a Coulomb-repulsive center having a potential barrier.

Very slow traps

The deeper the trap level the higher the trap characteristic time. For example, $\tau \approx 1.5s$ for $E_t = 0.7eV$ and $\sigma = 10^{-14} cm^2$. But the capture cross section is another factor that can make a trap slow or even "very slow". We will discuss here two possible mechanisms for the extremely slow capture rate, hence very low capture cross section. Both are based on the essentially inhomogeneous distribution of traps, namely traps gathered in clusters or traps belonging to the grain boundaries in polycrystalline materials.

Cluster model

The cluster model proposed in [36] for $\alpha - Si$ was recently used for very slow capacitance transients in CuInGaSe$_2$/CdS cells [37]. It is usual to determine σ from DLTS by measuring the density of trapped charge N_f as a function of trap-filling pulse time t_p. Common theory predicts the dependence

$$N_f(t_p) = N_t \left[1 - \exp\left(-\frac{t_p}{\tau_t} \right) \right]$$ (2.22)

with saturation on the N_t level when all traps are filled. In [37] unusually long pulses were used, up to $\sim 10^3 s$. Measured change in capacitance indicated trapping of majority carriers and demonstrated a logarithmic growth with pulse length in the five-decade range of $\sim 10^{-3} s \leq t_p \leq \sim 10^2 s$. An apparent saturation of the signal occurred only for $t_p \geq 10^2 s$. The explanation, as in [36], is that the potential barrier for free carriers created by the collective action of closely spaced charged traps is much higher than that for a single trap. This barrier increases with the trap filling in the cluster, providing stronger repulsion of carriers and reducing

the effective capture cross section. Theoretical analysis of the model leads to an equation that fits the experimental results in [37]

$$\frac{\Delta C}{C_o} = A_o \ln\left(1 + t_p / t_o\right) \qquad (2.23)$$

where $A_o = \dfrac{kT}{2N_t \cdot e \cdot f}$; $t_o = \dfrac{2A_o}{n_o \cdot \langle v_{th} \rangle \cdot \sigma_t}$; n_o is the free carrier density beyond the region occupied by the cluster potential. The cluster potential is $\Phi = N_s \cdot f$, where N_s is the density of carriers captured at $t = t_p$, and f is the model-dependent coupling factor. Theory also fits the data previously obtained for α-Si solar cells, $Ge_{0.3}Si_{0.7}/Si$ heterojunctions and plastically deformed GaAs (see references in [37]). For $CuInGaSe_2$ cells of various In/Ga ratios studied in [37], the t_o values were in the range of 10^{-4} to 10^{-2} s. Trap densities determined from the region, where $\Delta C(t_p)$ saturated, were rather high, from $4 \cdot 10^{15}$ to $\sim 2 \cdot 10^{17} cm^{-3}$, close or greater than the "C-V doping level". Assuming uniformly charged spherically shaped clusters of radius R (coupling factor $f = eR^2 / 3\varepsilon$ f), the authors estimated $R \approx 9 - 55 nm$ and $\sigma_t \approx 4 \cdot 10^{-22}$ to $3 \cdot 10^{-23} cm^2$. The authors recognize that the capture cross sections are surprisingly small but they have not yet proposed an unambiguous explanation.

Grain boundaries (GB)

It is mentioned in [37] that "the calculated radial dimensions of the hypothetical charging spheres are of the same order of magnitudes as the smallest polycrystalline 'grains'... This dimensional coincidence may imply that the charging is taking place at the surface of the grains."

We have recalculated the radius values using the same data and found that they are of the order of hundreds of nms, which makes the grain boundaries model even more probable. However the analysis carried out in [37] for the charged spherical trap clusters, should be revised with respect to two dimensional grain boundaries. We have done that and made some estimates for CdTe based on the information we obtained previously when studying the GB electronic properties in CdTe thin films [38-40].

The CdTe films were deposited on glass substrates at IEC (physical vapor deposition) and FS (vapor transport deposition). Some films were treated with CdCl$_2$ and doped with Cu at CSM. We also studied films prepared at NREL with a close space sublimation method. Those films were deposited on CdS/TCO/glass substrates and underwent a standard postdeposition treatment. Then they were lifted-off from the device and mounted on a glass substrate.

By using impedance spectroscopy [39-40] we were able to separate and independently study individual contributions of grain boundaries (GB) and intragrain (IG) material in film resistance and capacitance: R_{GB}, R_{IG}, C_{GB} and C_{IG}. Common major results for all films:

- The R_{GB} values are orders of magnitude greater than R_{IG}.

- Positive charge captured by grain boundary states provided a potential barrier for holes. The estimated barrier height Φ varied in dark from 0.3 to 0.8eV depending on post-deposition treatment and doping.

- Illumination could decrease R_{GB} significantly by reducing barrier height.

- Doping with Cu reduces dark R_{GB} by more than two orders of magnitude. Potential barrier thickness W (depleted thickness) estimated from capacitance was of the order of 200Å in the Cu-doped films.

- Space charge density in the depleted layer adjacent to GB calculated based on Φ and W turned out to be very high: $\rho/e \sim 10^{17} cm^{-3}$, sometimes up to $10^{18} cm^{-3}$. This indicates that the doping level $N = N_A - N_D$ in vicinity of GBs is much higher than in the grain bulk. The same result was obtained in [38] from measurements and modeling of the $R_{GB}(T)$ dependencies.

- Integrated density of charged states per unit GB area D_{GB} estimated from the $C_{GB}(V_{bias})$ studies is in the range of $\sim 10^{12} cm^{-2}$.

The following important conclusions from these results are relevant to the problem of slow traps and their contribution to the transients observed in CdTe cells:

- The GB state density per unit volume N_{GB} is high. For cube-shaped grains with a grain size d, $N_{GB} = 3(D_{GB}/d)$. That provides $N_{GB} = 3 \cdot 10^{16} cm^{-3}$ for $d = 1 \mu m$ and $D = 10^{12} cm^{-2}$.

- The GB repulsive potential barrier makes the capture cross section (CCS) for holes very low. CCS for a single deep state in the neutral GB, σ_{GB}^o, should be multiplied by a Boltzmann factor $\exp[-\Phi/kT]$ for electrically charged GB with a potential barrier height of Φ. For example, assuming $\sigma_{GB}(\Phi = 0) \approx 10^{-16} cm^2$ (reasonable value for the neutral defect), we obtain $\sigma_{GB}(\Phi = 0.3eV) \approx 1 \cdot 10^{-21} cm^2$ and $\sigma_{GB}(\Phi = 0.5eV) \approx 4 \cdot 10^{-25} cm^2$ at room temperature.

- Since the potential barrier increases with the density of charged GB states, N_{GB}^*, the capture cross section, hence the capture rate, reduces rapidly with the number of trapped holes. For a charged plane (like GB), $\Phi \propto Q^2 = f \times (eN_{GB}^*)^2$. A small change in the amount of trapped holes provides a small change in the barrier height of

$$\delta\Phi \approx 2\Phi(N_{GB}^*)(\delta N_{GB}^* / N_{GB}^*) \qquad (2.24)$$

Thus, if we start with $\Phi = 0.5eV$ and then increase density of trapped holes by 10%, the potential barrier grows by 0.1eV and the capture rate decreases 50x at T=300 K. A 20% increase will reduce the rate about two thousand times. That means that we should not expect any significant change in the GB states occupation in a reasonable time of observation of capture process, say in hours or even days.

- It is easy to show that the kinetics of trap filling for reasonable time (small changes in N_{GB}^*) is described by the equation similar to Eq. 2.23: $N_{GB}^*(t) \propto \ln[t/t_o + 1]$. That increases the probability that the long term transients in capacitance observed in CIGS cells in [37] really were due to filling GB states.

- The potential of the positively charged GB is repulsive for holes but attractive for electrons. Therefore the GB CCS and the capture rate for electrons is orders of magnitude higher than for holes, as seen in our studies of photoconductivity of CdTe polycrystalline films. Conductivity increases rapidly and greatly with illumination, due to the reduction of the potential barrier caused by a decrease in the GB positive charge. The latter is provided by capturing of photogenerated electrons that recombine with holes trapped by GB states. After

the light was switched off, restoration of the film resistance takes hours. In a wide time range (from ~10s and not close to saturation) the time dependence of the resistance change is $\Delta R \propto \ln t$ which means that slow capturing traps is the major mechanism of potential barrier restoration. The rate of capturing reduces with time of observation.

- These are all grounds to expect manifestation of the GB deep states in transients measured on CdTe solar cells. Analysis of the data will probably be complicated due to presence of both hole and electron capture/emission processes. We must remember that GB provides acceptor-like and donor-like states in the gap, thus hole- and electron-traps. Detailed studying of transients can provide additional information about the GB electronic properties and their dependence on cell processing and degradation. It would be useful to compare results of studies on cells with those conducted on CdTe films, especially extracted from the cells with the lift-off technique.

2.3.4 Transients.

In previous sections we considered transients mostly as an additional tool for detecting and studying deep states. But the problem could be viewed from another, more fundamental, side. What are the mechanisms of transients in electrical and photoelectric characteristics that were being observed in CdTe cells for a long time but not studied thoroughly so far? Can studies of transients provide better understanding of basic issues behind cell performance and stability, for example, identify the defects effecting electronic properties of a cell, migration and mutation of these defects, their influence on cell degradation, etc.?

Strong support to the necessity of the systematic transient studies is provided by recent discussion of this subject (March 2002) initiated by Ken Zweibel. E-mail messages exchanged between members of CdTe team (26 messages in a week) helped to better understand the current status of transient studies in CdTe, to discuss definitions, in particular the terms "transients" and "degradation", to formulate the problems, and discuss some possible approaches to their solution. It seems appropriate to include in the discussion below some quotations from the messages.

One problem is the influence of transients on cell characterization results. Since it is impossible to avoid the effect of transients, we must develop the procedures of measurement and

data treatment that minimize their impact. As a first step, the CdTe Team needs to standardize conditions of measurements, which will make comparable the results obtained at various facilities. Ken Zweibel wrote in his initial messages (March 22, 2002):

> "…I have been concerned about transients - those that disguise electronic measurements like IV and capacitance; and those that disguise instability issues by making efficiency measurements irreproducible. …I just want to be sure that everyone is on the same page about them in terms of being aware of their potential to distort measurements. …if we don't conscientiously avoid them, they will hurt our data. … In my view, a transient is a short-lived, mostly reversible phenomenon that is probably due to filling/emptying traps under bias and light. … transients are reversible (up to a point, perhaps) and they can influence measurements by about 20%, maybe more. …One of the key observations that motivated the use of the term 'transient' was that if a module/cell were measured at max power (after a sufficient interval << day) it would NOT show the transient. Thus a baseline measurement was developed (max power tracking) that obviated the transients that would otherwise occur if pulse simulators were used, or if the module were swept right after being either outside in the sun under various circumstances or indoors with its wires crossed, etc. In that sense, it is like saying that standard conditions include not only temperature, but device prehistory as it might impact its electronic state."

Transients manifest themselves not only in J-V characteristics. As examples we can mention the problem of C-V profiling in the presence of slow traps considered in Sec.2.3.1 or transients in conductivity of thin films (Sec. 2.3.3). Before developing standardized procedures of measurements and data treatment we need to study in detail and better understand transients of various characteristics of devices and materials we are interested in. An active discussion of definition of transients was not about terminology itself.

K. Zweibel: "In themselves, they $\langle transients. - V.K. \rangle$ are very interesting phenomena" !!

In the course of discussion more fundamental issues were touched. What are the mechanisms of long term changes in the cell characteristics caused by external factors: light, bias, temperature, etc.? Is it reasonable and possible to separate long-term changes in a cell into well distinct categories: transients and degradation? Is reversibility a good criterion to define transients? Some participants of the discussion expressed opposite opinions on this subject, e.g.:

> C. Ferekides: "Anything completely reversible should be considered a transient, and everything else i.e. partially reversible etc. a degradation".

> J. Sites: "If a cell shows performance changes in the light, or following bias, but all parameters return to initial values after a reasonable period, say overnight, in the dark at zero bias, I would call that a transient. In my experience, there are at least some CdTe transients that occur independently of any degradation."

B. von Roedern: "I strongly suspect that degradation and transients are related. In a-Si and CdTe, "initially reversible" degradation (transients) may develop into (more or less severe) irreversible degradation. I argue that both transients and degradation are driven by carriers and that carrier induced diffusion or structural changes will eventually stabilize the mechanism that is initially electronic ("trapping"). If transients and degradation turn out to be related, any approach attempting to separate the problem into degradation and transient mechanism would be the wrong approach to the problem".

Less categorical statements:

Peter Meyers: "…the differentiation between reversible and irreversible is not always clear. That is, a mechanism - such as filling or emptying of traps or defect mutation - may be completely reversible on a microscopic level, but in practice the effect of those microscopic changes on degradation modes may not lead to restoration of the original device performance."

A. Fahrenbruch: "… "reversible" in the lab may be different than "reversible" in the field. In the lab the photo-induced degradation can be reversed by dark annealing, while in the field it generally can't be."

V. Karpov: "My question was whether the system has just two distinctive relaxation times (defect lifetime and that of transient) or it has a continuous spectrum of relaxation times spanning from, say, microseconds, to years? In the former case it is natural to discriminate between the transients and defects. In the latter case it would be a matter of definition."

It is seen from the quotations above that the effects caused solely by changes in trap occupation were discussed as well as those due to the atomic, structural defects, their generation, mutation and migration, and also combination of these mechanisms. Discriminating these two mechanisms is an important but not simple problem, and cannot be solved based only on significantly different characteristic times of the processes or their reversibility. For example,

V. Karpov: "…if traps are distributed continuously in energy, their relaxation (trapping - detrapping) times form exponentially wide distribution, which may show up in transients. It may also have to do with degradation if adding the electron to the trap generates lattice distortion strong enough to transform it into a defect (such mechanisms have been suggested in the literature)".

A. Fahrenbruch: "Two items to add to the list of reversible transients are: (a) reversible local atomic configuration changes driven by carrier occupancy (e.g., metastable defects in a-Si:H, reversible optical degradation in CdS, DX centers in GaAs, "H alpha 2" defects in p-Si) and, (b) phase changes [e.g., driven by changes in x and/or T for $Cd_{(1-x)}Te$].

However, the situation does not seem totally hopeless: some possible approaches to discriminating were proposed, e.g.

J.Sites: " (2) General mechanisms that can alter cell performance: (a) Long-lived electronic states (atomic structure stable). (b) Diffusion of atoms. (c) Field driven movement of atoms. (d) Atoms moved by currents or hot spots. Any others? Obviously combinations are possible.

(3) Intuitive thoughts: (a) Transients are unlikely to be caused by 2b or d, since you would not expect them to relax to the initial state. 2c by itself is unlikely, since the internal field is never reversed. Does that leave an alternative besides 2a? b) Transients and degradation almost certainly involve different mechanisms, since empirically voltage goes up with transient changes and down with degradation. (c) Cell changes almost certainly have spatial variations, since all the mechanisms under (2) vary between grain surfaces and interior. All the experiments I know about confirm this. (d) There are experiments that can test which mechanisms are operative: temperature variation (diffusion), bias variation (field), capacitance (states), deliberate weak spots, tracking micro-nonuniformities. (e) Separation of mechanisms is messy, cannot assume that mechanisms combine linearly, and is not convincing unless multiple parameters are tracked simultaneously.

(4) As Bolko points out, location is also critical, so his strategy of systematically altering front or back (and I would think including SIMS in the measurements), makes a lot of sense to me. Sounds like a good reason to have a team!"

The discussion has shown that the whole team considers transients in CdTe cells as an important problem that should be addressed in our studies. At the same time it was mentioned more than once that there has been a lack of studies of this kind and information we have is far less complete and detailed than say for amorphous silicon. The only publications on CdTe we have found are those by Sasala & Sites [32, 33] and by MacMahon [34]. All three are devoted to transients in J-V characteristics at varying temperature due to light or bias switch. Some non-systematic data on capacitance transients can be found, mostly on hysteresis in C-V profiles.

Numerous publications on capacitance transients in amorphous silicon provided vast information on metastable effects/defects in amorphous silicon. Capacitance transients are mostly due to slow changes in the space charge density after switching bias or light. Therefore interpretation is easier than for transients in J-V dependencies or photoconductivity. From the magnitude of change in capacitance one can estimate the charged defect density, no matter whether these changes are due to change in filling existing traps or generation of new atomic/structural defects. The sign of the transient allows discrimination of majority- and minority-carrier traps. The capacitance magnitude and time dependence studied at various temperatures provide the characteristic time of traps, their energy levels, capture cross section, concentration or DOS function in the case of continuous distribution of states. If transients are due to generation of new defects or their mutation, the activation energy of the processes can be derived from the $C(t,T)$ dependencies. In Sec. 2.3.3 we have discussed specific kinetics of GB

boundary filling. Hopefully it will help us to identify and estimate the GB contribution to the capacitance transients.

Capacitance transients are an important part of the studies we started recently, inspired in part by the discussion we quoted above. But also transients in J-V, C-V and C-f characteristics will be studied in parallel. Combining various effects and their simultaneous analysis/modeling, hopefully will provide more reliable and detailed information on mechanisms of transients and cell degradation. These studies of as-prepared and stressed cells accompanied by spectrally and spatially resolved EL, PL measurements (See Sec.1) , TCM (see Sec.3), NSOM [11,40], are expected to promote our knowledge and understanding of defect in CdTe cells that control their electronic properties, hence performance.

We hope that these basic studies combined with intentional variations in deposition and postdeposition procedures, in kind, amount and method of introducing of dopant, and accompanied with structural and compositional studies, can also provide significant progress in identification of defects responsible for specific electronic states. The current situation is far from being perfect. Indeed, in many cases different authors attribute the same (or almost the same) energy level to different defects, even if the level is determined with the same method, say DLTS. Conversely, different levels are ascribed to the same defect. Frequently, a significant discrepancy is seen in the energy of the same state/defect obtained by measurements and theoretically. A good example is a variety of energy levels ascribed to the Cu substitute for Cd. It should be mentioned that the problem of identification is even more severe for the polycrystalline CdTe, where manifestations of the same defect can differ to some extent for location in the grain bulk and in the GB region.

2.4   New Measurement System

To realize our new program of studying deep states with electrical methods a new measurement system has been built. It is designed to provide admittance spectroscopy (AS) measurements at different biases, capacitance-voltage profiling (CV), current-voltage characterization (JV) , and measurements of transients in all characteristics listed above (Tr). All measurements can be conducted at various temperatures, in dark and under illumination.

The experimental 'parameter testing space' for the admittance measurements (AS, CV, Tr) covers five dimensions:

1. AC current frequency from 25Hz to 30MHz

2. DC Bias from −3V to +3V. A wider range can be used at the risk of damaging the sample.

3. Temperature ranges from −190°C to +80°C. We can maintain sample within one °C for 10 minutes and for a longer time at temperatures near room temperature.

4. Light of intensity up to 1 Sun is injected through fiber cable. Spectral content is varied using filters.

5. Sampling time ranges from the shortest interval of about 1.5 seconds to about 600 seconds (keeping temperature within one degree C). It is possible to sample up to several days at room temperature.

AC Current and DC Bias

The AC current and DC bias are provided by a HP 4284A and an HP4285A Precision LCR Meters. The HP 4284A has an AC signal frequency range of 20Hz to 1MHz and the HP4285A a range of 75kHz to 30MHz. In addition to the AC signal, a superimposed DC bias can be applied. These instruments are programmatically controlled using HP-VEE software. They are configured to report out the absolute value of admittance and phase angle shift. From these, values such as capacitance, conductance, and resistance for both parallel and serial equivalent circuits are calculated.

Temperature

A custom designed sample stage was built with the principal goal of providing thermal stability. This is achieved through an insulated copper chamber with a large (15kg) copper mass. The high heat conductivity of copper reduces thermal gradients within the chamber and the large mass (heat capacity) provides thermal stability for the time sufficient to perform each type of measurement at practically constant temperature. The chamber is heated or cooled beyond the testing temperature(s), allowed to settle, and then as it slowly (about 0.1 °C per minute or slower) returns to room temperature, tests are programmatically triggered at preset temperatures.

Temperature is monitored using a K-type thermocouple connected to an Omega I-series controller which is in turn connected to a PC through a RS232 port.

Sample Stage

The sample rests on 5cm x 5cm glass rectangle that allows illumination from underneath. The back contact and front contact sample probes are Cu-Tin-Zinc alloy, shaped to have an approximately 1mm^2 flat surface for contact with a sample. They are mounted on a custom-built spring cantilever that is controlled with a set screw. The sample itself is located within a 5cm diameter by 5cm high copper cylinder inner chamber. The chamber has notches to allow the probes access to the sample. This inner chamber reduces convection around the sample and helps stabilize the temperature and reduce thermal gradients.

The inner chamber is enclosed in an outer chamber consisting of copper sheets and 2.54cm (1 inch) thick copper slabs. This outer chamber weighs 15kg and provides thermal mass to stabilize the temperature in addition to screening out electromagnetic noise. It is grounded to the LCR meters. The chamber is encased in three layers of insulation foam board with a total thickness of 11.43 cm (4.5 inches).

Heating and Cooling

Heating is provided by four 6.4mm (¼ inch) by 11.4cm (4.5 inch) 35W cartridge heaters (140W total). These are inserted into bored holes in the copper slabs. The sample can be heated up to 80 °C. This upper limit is because of the melting temperature of the foam board insulation which is less than 100 °C.

Cooling is provided by pumping liquid nitrogen through 6.4mm (¼ inch) diameter copper tubing that is wrapped around the outer chamber copper slabs. The sample can be taken down to near liquid nitrogen temperatures.

Light

Light is conveyed to the sample through the insulation and copper chambers with a fiber cable 1.25cm (1/2 inch) in diameter. The light source is provided by a Fiber Lite A240P power supply and the accompanying Fiber Lite A240L 150W light source. An intensity of up to about 1 sun is possible. Band pass filters can be inserted to control the wavelength from 500nm to 950nm.

Time

The fastest LCR meter trigger response time is 1.3 seconds. A sampling length of 600 seconds is possible within a temperature range of 1C (heating/cooling temperature gradient of 0.1C per minute). At room temperature, tests can be run for several days for studying long-term transients.

Thermal IV characterization

The copper sample stage can also be used to generate J-V curves in a wide temperature range, the same as for admittance measurements. The most desirable approach is to reroute the contact leads to a Keithley source meter and to run the appropriate HPVEE driver program. However, access to a Keithley source meter is limited. Therefore, an alternate system has been developed using the LCR meter as a DC power supply and an available Keithley Digital Multi Meter. Unfortunately, to date, the J-V curves generated in this manner have been of inferior quality. This problem will be addressed as time permits. Currently we measure J-V characteristics at room temperature with a separate system that allows observation of transients caused by the light pulse and bias voltage switch. The time of transient observation is up to hours.

2.5. Experimental Results

In this section we present some results obtained recently with the new system described in Sec.2.4. Measurements were conducted on the CdS/CdTe cells supplied by Dr. D. Albin (NREL). CdS layers were prepared with the chemical bath deposition technique, and CdTe with close space sublimation. For these first tests a wide range of processing conditions was examined (Table 2.3).

Table 2.3

Cell ID	SnO_2 type	CBD CdS time, min	CSS O_2 press., torr	CdTe thickn., μm	$CdCl_2$ treat. time, min	Pre-contact. etch
D131A	Bilayer	35	0.8	8.9	10.0	Std. NP
D133D	Bilayer	37.5	0.8	9.0	10.0	Std. NP
D135B	Bilayer	40	0.8	8.3	10.0	Std. NP
D114B	Single l-er	35	1.0	8.5	15.0	200:50BrM
D117A	Bilayer	35	1.0	8.7	15.0	200:50BrM
D115B	Bilayer	35	0.8	9.7	6.0	200:50BrM
D116D	Bilayer	35	0.8	9.1	13.5	200:50BrM
D217C	Bilayer	37	0.8	9.2	8.0	200:50BrM
D220B	Bilayer	37	1.4	8.8	7.0	200:50BrM

J-V dependencies measured at CSM demonstrated close efficiency values, except cell D131A that has obvious shunting effect and was excluded from further measurements. The results of admittance measurements presented below were selected to illustrate the major statements and proposed approaches in Sec. 2.3.
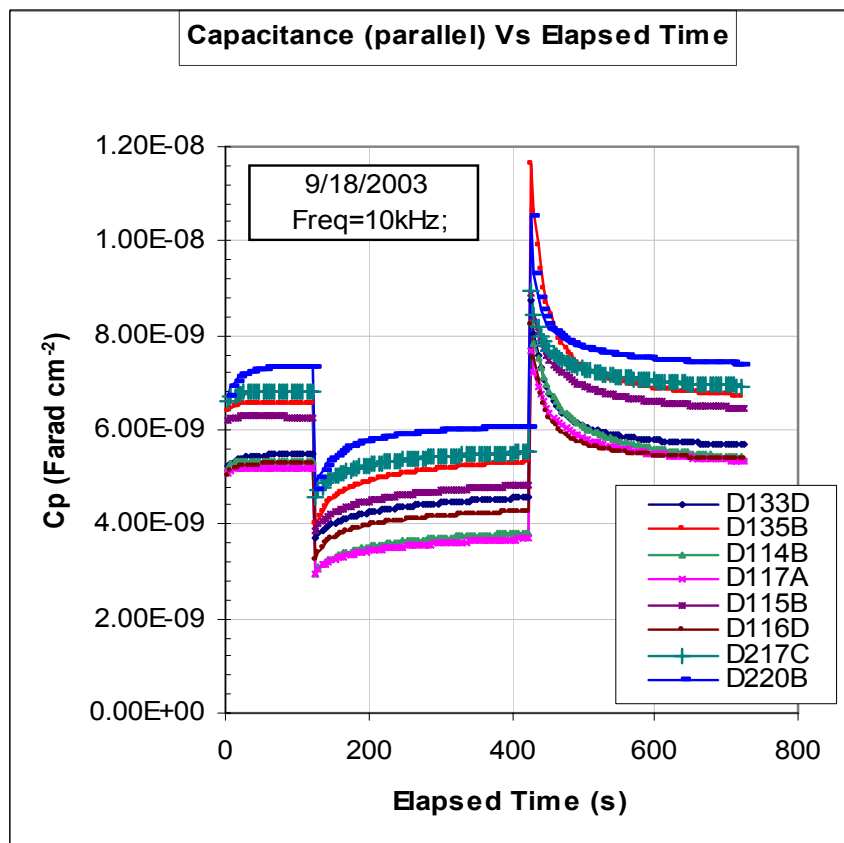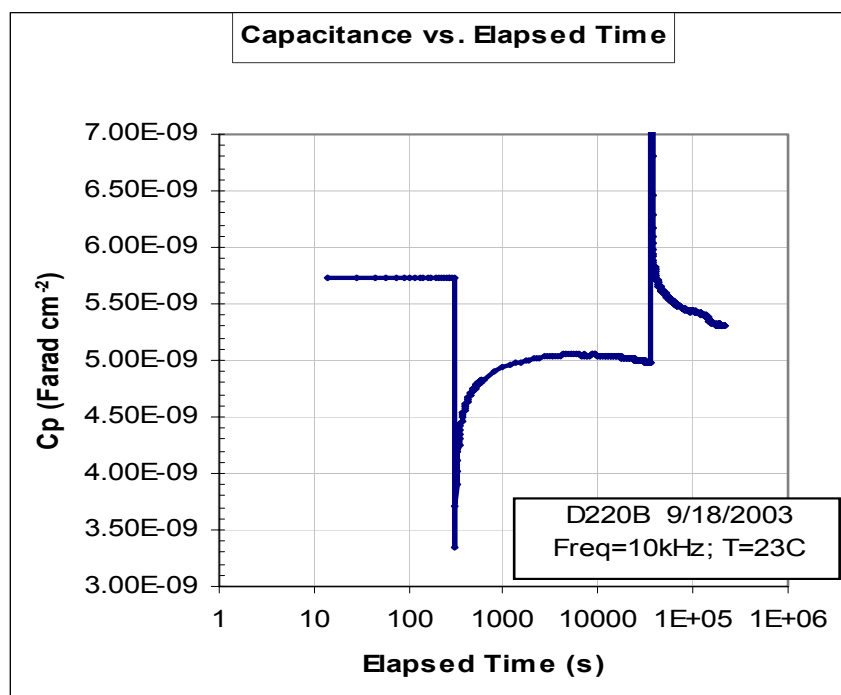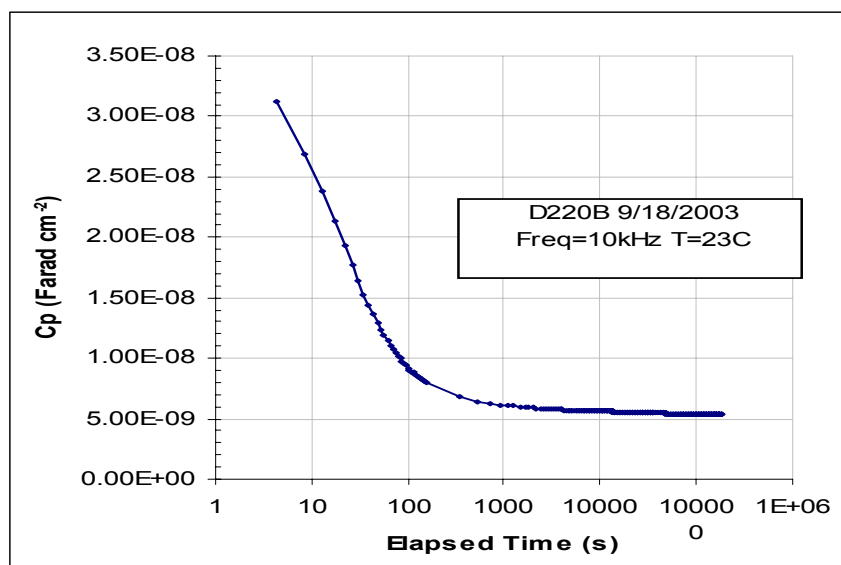
Fig. 2.7. Capacitance transients at T=23°C for the samples listed in Table 2.3, except D131A. The bias voltage sequence is: 0 V → -1 V → 0 V

As seen in Fig. 2.3, the capacitance transients of significant magnitude are observed for all cells. As mentioned in Sec.4, the LCR meter trigger response time is in the range of seconds, therefore we lose the capacitance transients with characteristic times in the range below several seconds. Arrangements with Dr. D. Young (NREL) will allow use of equipment that allows observation and measurement of transients at much shorter time if needed. More detailed studies of admittance, including capacitance transients were conducted on the cell D220B. In particular, transients were measured over a much longer time range up to $t = 2 \cdot 10^5 s$ (~55 hours). The results are presented in Fig. 2.8 with a logarithmic time scale.

(a)

(b)

Fig. 2.8 Capacitance transients at T=23°C for the cell D220B in a wide time range.
(a) The bias voltage sequence is: 0 V → -1 V → 0 V; (b) after switching back to V= 0

As shown by these initial tests long-term capacitance transients were observed that required several days for total recovery of the initial capacitance.
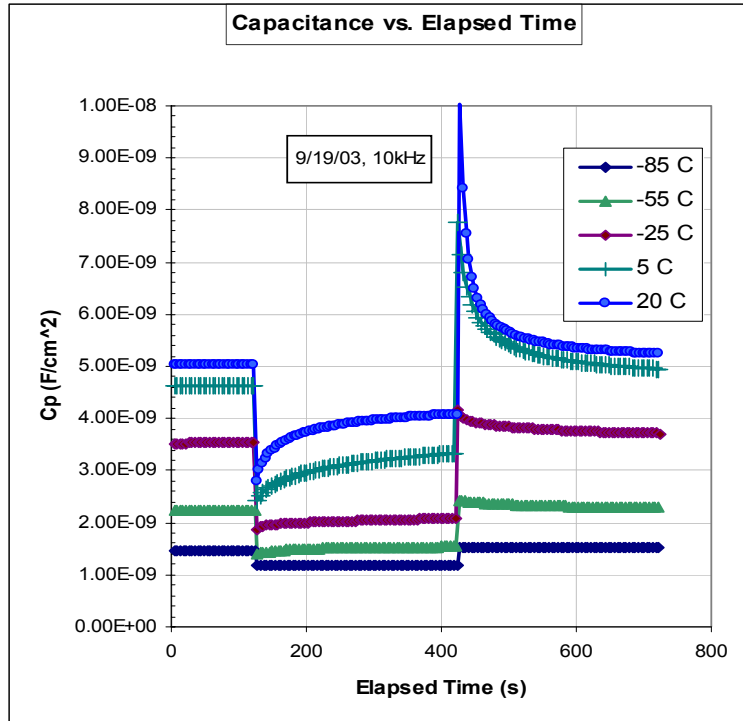
(a)
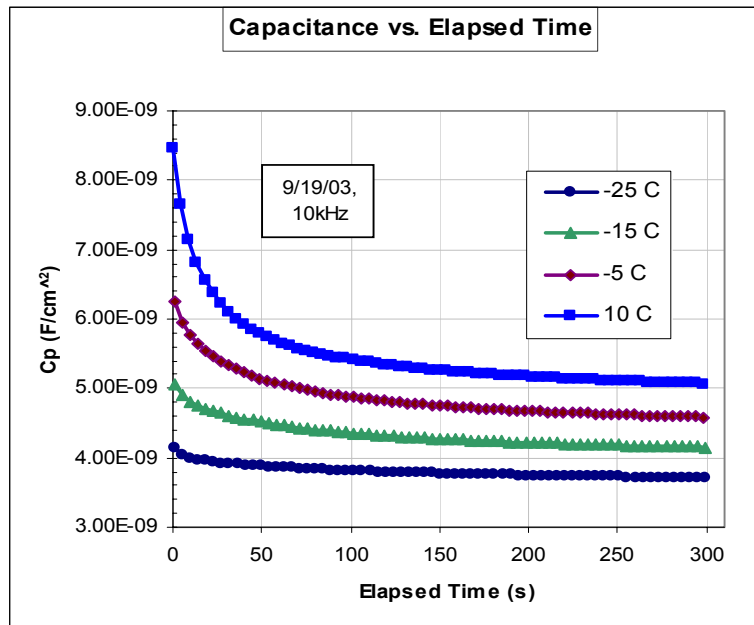
(b)

Fig. 2.9 Capacitance transients at reduced temperatures for the cell D220B.
(a) Bias voltage sequence: 0 V→ -1V → 0V; (b) expanded view following return to 0 V.

The evolution of capacitance transients with cell cooling is illustrated by Fig. 2.9a. Fig. 2.9b shows separately transients after voltage switching back from -1 V to 0 V. Curves show a decrease in magnitude and in the rate of capacitance change with cooling. To find possible manifestations of the single trap levels or narrow bands, we analyzed the DLTS function $S = dC/d(\ln t)$ at each temperature. According the simple theory, the dependencies $S(t)$ or $S(\ln t)$ should have a peak at $t = \tau$ where τ is the characteristic time of the trap. As seen from Fig. 2.10 the peaks were observed at all temperatures in the range tested. Position of the peak, hence the τ value shifted toward longer times with cooling. With a common procedure of $\tau(t)$ analysis, using the Arrhenius plot, we have estimated activation energy of the trap level $E_a = 0.39 eV$ and capture cross section, $\sigma_\infty = 10^{-20} cm^2$. When cooling to -70 ^{o}C we have found another trap state: { $E_a = 0.42 eV$; $\sigma_\infty = 10^{-18} \cdot cm^2$ }. It should be mentioned that so far we did not try to separate contributions in activation energy of the trap level energy and potential barrier for capturing, therefore the capture cross section derived from Arrhenius plot is denoted as σ_∞.
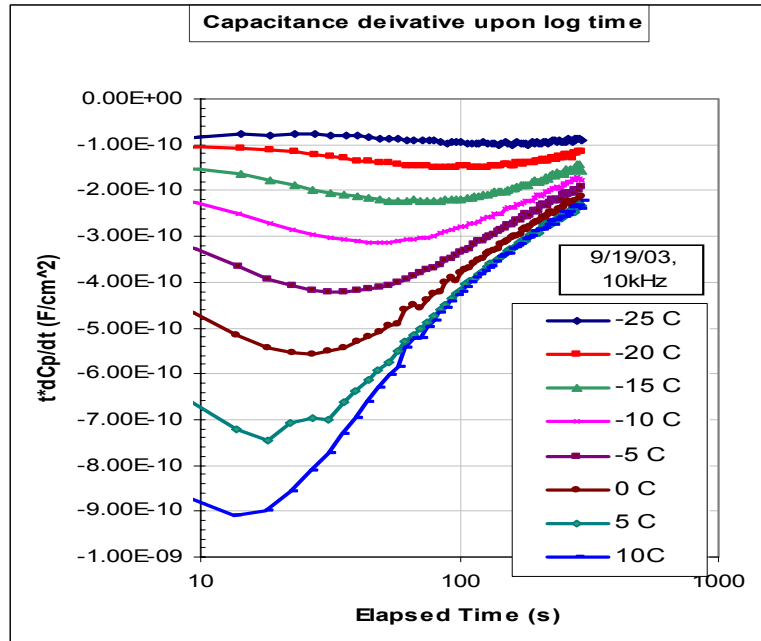

Fig. 2.10   DLTS function for the capacitance dependence on time after the voltage switch from -1V to 0 V, in the temperature range of 10°C to -25°C. Cell D220B.

A similar analysis of the transients after voltage switch from 0 V to -1 V revealed two more levels: { $E_a = 0.47 eV$; $\sigma_\infty = 10^{-16} \cdot cm^2$ } and { $E_a = 0.88 eV$; $\sigma_\infty = 10^{-12} \cdot cm^2$ }.

Fig. 2.11 shows capacitance transients for the cell D217C at elevated temperatures on a logarithmic time scale. As expected, both magnitudes of transients and the rate of change increased with higher temperature. The data for the short times after switching voltage to -1 V are not available as explained above. Therefore we were not able to search for relatively "fast" states with $\tau \lesssim 1s$. But evidence of the slower state can be seen at longer times. The tendency to saturation in the C(t) dependence is seen for the reverse bias applied as temperature increases. For the highest temperatures of measurements (70, 75, 80°C), saturation is followed by the additional increases.
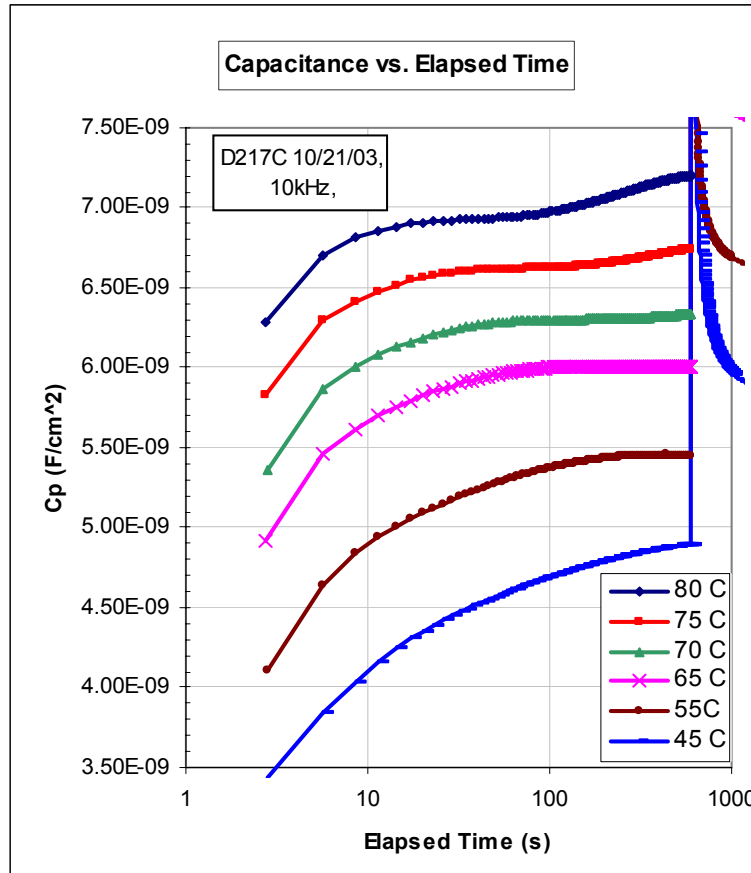
Fig. 2.11. Capacitance transients at elevated temperatures for the cell D217C.

71

The DLTS function analysis reveals peaks in the S(t) dependence (see Fig. 2.12) whose position on the time scale rapidly shifts with temperature. Probably this can be considered as evidence of presence of a new level with high activation energy. Unfortunately, measurements at elevated temperature were not as long as at the room temperature, but extension up to 10^4 s is planned for the nearest future.
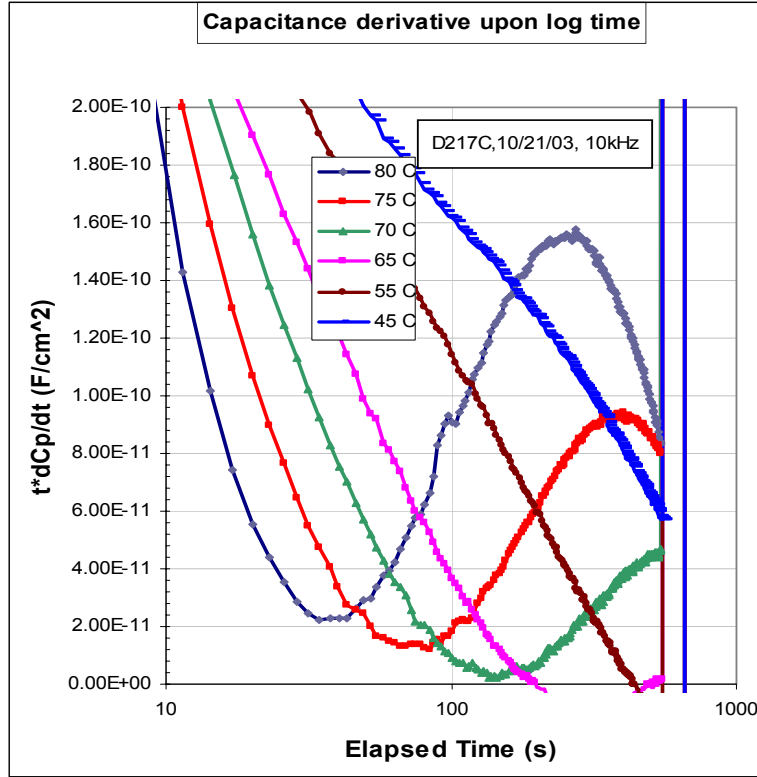
Fig. 2.12.   DLTS function for the data presented in Fig. 2.11.
The S(t) peaks are well seen at T >70°C indicating presence of a single trap level/narrow band.

Concluding with transients, it should be mentioned that all the states detected so far from the transient analysis did not reveal themselves in our AS measurements because their characteristic frequencies, $\omega_t = \tau^{-1}$ at reasonable temperatures are beyond the limits of LCR meters. We have not yet studied the long-term transients ($\tau \sim$ hours) at elevated and reduced temperatures although it is very probable that they would provide an opportunity to detect and study more trap levels.

At long times of observation, transient demonstrate very slow changes, maybe caused by specific capture-time dependence due to collective action of closely distanced traps (grain boundaries, or trap clustering). We have not yet analyzed very long-term transients already measured at room temperatures, or attempted to derive the trap concentration from the magnitude of transients. Our future studies will examine this, as well as analysis of differences in transients measured on cells with varying processing procedure and also caused by stressing.

We have also measured C-f and C-V profiles on all cells. In selected cells we measured these characteristics at varied temperatures. On those C(f) and G(f) dependencies demonstrated a peak in the range of ~ 100 kHz or lower at lower temperatures and higher at the elevated temperatures. The Arrhenius plot in the temperature range of 220 K to 340 K provided an activation energy of 0.32 eV and capture cross section of ~10^{-16} cm^2. So far this is the only "fast" state we have detected by AS.

Both C-V and C-f dependencies manifested a significant variation with temperature. Figs. 2.13 and 2.14 illustrate changes at enhanced temperatures.
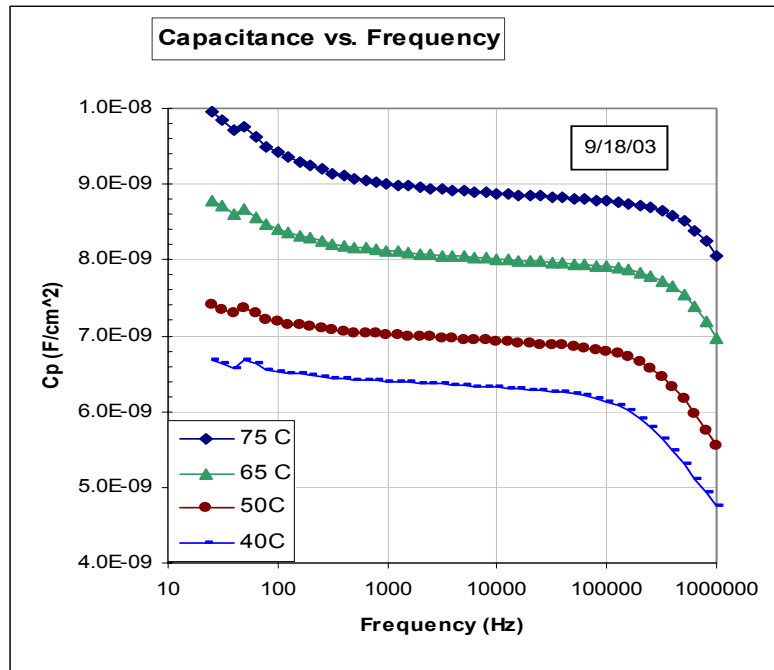

Fig. 2.13.   Variation of the C-f dependence with varying temperature
at the elevated temperature range. Cell D220B.
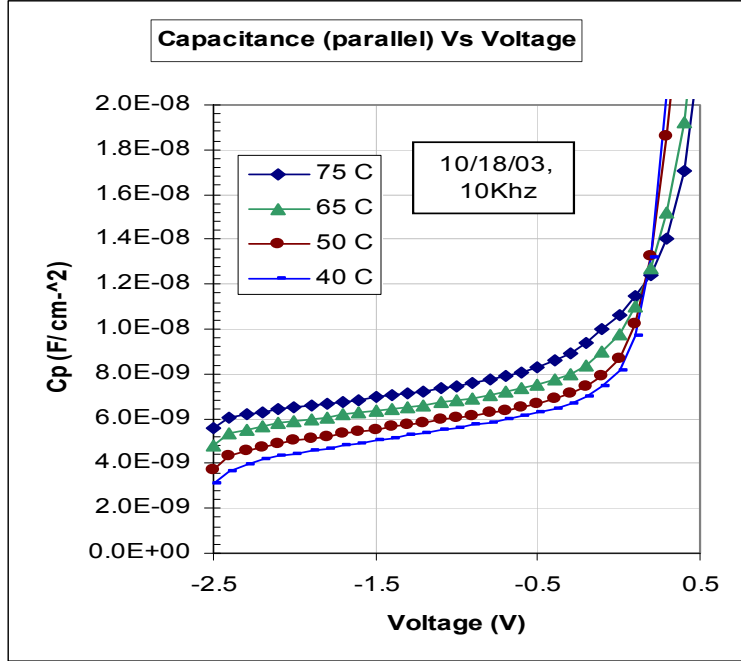
Fig. 2.14. Variation of the C-V dependence with varying temperature at the elevated temperature range. Cell D220B.

The temperature range of these measurements was extended down to -130°C. Capacitance continually decreased over the entire temperature range. For example, its value measured at $V_{bias} = 0$ and f = 10 KHz, decreased 4.2 times from T= + 80°C to T= -130°C. These data can be explained partially by greater contribution of the oscillating trapped charge in measured capacitance due to the exponential decrease in characteristic time with temperature. However, the free carrier freeze-out effect cannot be excluded. We are planning to continue detailed measurements as well as to model capacitance with the SCAPS program keeping in mind clarification of the role of the two mechanisms. In particular, if considerable contribution of the second effect is found, that would indicate a significant role of the not too shallow states in controlling carrier concentration. In turn, it will bring us again to the problem of concentration of the Cu_{Cd} defects and their compensation, as well as of the origin of the state with $E_a = 0.32eV$ detected by AS measurements. Is not the same defect is responsible for this state?

74

2.6 SUMMARY

1. The basics of admittance spectroscopy (AS) as a method for detection of deep states and studying their properties were presented and discussed along with two modifications of AS. (Sections 2.2.1 and 2.2.2)

2. Our studies of CdTe cells using AS and modified AS revealed various deep states with concentration, spatial distribution and characteristic time, that depend on deposition technique, postdeposition treatment, and contacting procedure (Sec. 2.2.3). A common feature of the cells fabricated at different facilities (FS, NREL, UT, FS/CSM) was a high trap concentration, N_t, exceeding doping level, N_{C-V}, determined by C-V profiling. In some cells density of detected trap states was of the order of 10^{16} cm^3. Experimental data also indicated presence of significant amount of slower traps not detectable with the standard AS equipment .

3. The common approach to the analysis of AS and DLTS measurements is based on the theory valid for low trap concentration much smaller than the doping level ($N_t << N$). In the case of CdTe this approach should be revised based on more adequate theory and numerical modeling using more reliable physical models. The common equations used for trap concentration estimates, actually provide the ratio N_t / N. Analysis presented in Sec. 2.3.1 shows that at $N_t \gtrsim N$ this ratio is underestimated, especially if the levels are located close to Fermi level. On the other hand, the doping level derived from C-V profiling, N_{C-V} can be strongly overestimated if $N_t > N$. This problem is also analyzed in Sec. 2.3.1. Numerical estimates of apparent doping level, N_{C-V}, compared to the real one, N , are presented for CdTe with two trap levels having characteristics close to those determined by AS. These two levels are rather fast: $\tau_1 \sim \mu s$ and $\tau_2 \sim ms$. Because C-V profiling usually takes minutes or more, one can expect a significant influence of slower states, say in the range of seconds or minutes. This would increase the discrepancy between N_{C-V} and N.

4. Other problems are discussed related to detection and studying of deep states in CdTe. In Sec. 2.3.2 the technical limitations on the characteristic time of traps available for detection by AS are considered. As possible solutions of the problem, variation of temperature and measurements of transients are discussed. The procedure for determining trap cross section is

considered in Sec. 2.3.3, in particular with respect to the traps with the repulsing potential barrier. The latter is considered in more detail for the barrier provided by collective action of closely spaced traps, e.g., trap clusters and especially grain boundary states. The latter are considered as the most important origin of very slow traps. The trap filling dependence on time is specific for these "collective" trap states which can be used for their identification.

5. The usefulness and even necessity of studying transients in capacitance, J-V dependencies and photoconductivity is discussed in Sec. 2.3.4. The current state of these studies in CdTe is unsatisfactory. The transients have been observed but not studied properly. Studying of capacitance transients is the most promising method for detection slow/deep states, estimating trap concentration, distinguishing between the majority- and minority-carrier traps. Combined studies in amorphous silicon of capacitance and J-V transients caused by bias and light pulses proved to be a powerful method for detection and characterization of deep states and metastable defects.

6. A new measurement system recently developed in our facilities is described in Sec. 2.4. The system is designed for studying the cell admittance, in particular, C-f and C-V dependencies, along with transients in a wide temperature range, from below -100°C to +80°C. Measurements can be conducted in dark and under illumination of varying intensity and spectrum.

7. The preliminary results of measurements presented in Sec 2.5 show that the system provides the expected/designed options. Measurements revealed transients, including very long-term ones. Analysis of transients based on DLTS function detected at least five levels or narrow bands with characteristic times in the range of $\sim 10s - 100s$ not available for common AS. Analysis of temperature dependencies using the Arrhenius plot allowed estimates of activation energy and capture cross section. We noted very slow transients are seen, non-exponential decays, and very low capture cross sections that could be attributed to grain boundaries. A significant capacitance dependence on temperature in the range of -130 to +80°C was found. Possible mechanisms of dependence were briefly discussed.

3. SCANNING TUNNELING MICROSCOPY AND LOCAL SPECTROSCOPY OF THE BACK CONTACT INTERFACE

3.1 High Resolution Current Mapping at p^+-ZnTe/p-CdTe Back Contact Interface

A number of microscopic probes have been used successfully on polycrystalline solar cell materials. Examples are cathodoluminescence spectroscopy [7] and near-field scanning optical microscopy [11]. Under favorable circumstances these techniques can map carrier generation/recombination or impurity concentration with spatial resolution of about 100 nm. Scanning capacitance microscopy in an atomic force microscope has recently been used to determine the potential distribution at single grain boundaries, critical to charge collection and recombination [42]. A key device property, carrier transport across contacts and in the absorber itself, remains poorly understood, yet is crucial for optimizing the short-circuit current and efficiency of a solar cell.

We have demonstrated a novel technique, charge injection spectroscopy (CIS) in a scanning tunneling microscope (STM), which can provide detailed maps of carrier transport near the interface between the polycrystalline absorber layer of a thin film solar cell and an adjacent ohmic contact. We use this technique to image near-surface transport between a p-CdTe surface and a p^+-ZnTe back contact interface with lateral resolution below 20 nm, about 2 orders of magnitude below the absorber grain size. Charge transfer between the p^+-ZnTe contact and the p-CdTe absorber is highly non-uniform, and involves large areas with roughly constant high resistance coexisting with nanoscale high-conductance pathways. A majority of the cell current flows along these pathways, which are often localized at grain boundaries, thus highlighting an important role of grain boundaries as efficient near-contact transport channels. Conducting paths found within a few of the grains suggest that specific intragrain defects may also cause a lowering of the contact resistance. Identification and promotion of such beneficial defects could result in substantially reduced overall contact resistance.

The samples used were standard CdTe/CdS heterojunction structures in 'superstrate' configuration from First Solar, LLC (Fig. 3.1) with our standard ZnTe:Cu contact. STM

experiments were performed on the ZnTe surface layer under dark conditions and at room temperature, using a home made tunneling microscope operating in air or high vacuum. Electrochemically etched tungsten tips were used as emitters, while the STM collector contact was made to exposed sections of the SnO_2 cell front contact. In this configuration, we simultaneously measured the surface topography via constant-current STM and current-voltage (I-V) spectra on a regular grid of points across the field of view (FOV). From the measured I-V spectra, current values at constant bias voltage were extracted to produce high-resolution two-dimensional current maps, I(x,y). STM measurements were complemented by XTEM, performed in a Philips CM200 microscope at 200 keV beam energy, on samples prepared by tripod polishing and brief low-energy ion milling.

Fig. 3.1 illustrates the layout of our STM experiments. With emitter and collector contacts on opposite sides of the solar cell, carriers injected from the tip into the p^+-ZnTe contact layer have to undergo transport into and through the entire device structure to contribute to the overall current measured at the SnO_2 collector contact. Conventional STM on single crystals is surface sensitive, and contrast is usually dominated by surface states of the sample. On a highly heterogeneous polycrystalline device structure, additional contrast may arise if the overall local conductance of contact and cell is low, i.e., comparable to the conductance of the tunneling gap. Suppose, for example, highly insulating grains with a substantial potential barrier at the ZnTe/CdTe interface, separated by grain boundaries with higher conductance and locally reduced contact barrier. Carriers injected into the ZnTe layer above a grain [Fig. 3.1, position (1)] will then spread in the ZnTe to the surrounding grain boundaries, where they are transferred into the p-CdTe absorber and to the STM collector contact. The equivalent electrical resistance in this case is a sum of the tunneling resistance [R_t], the position-dependent resistance to carrier spreading in the ZnTe [$R_s(x,y)$], and the equivalent resistance of current transport across the contact and through the cell [R_c]: $R_{tot}(1) = R_t + R_s(x,y) + R_c$. If, however, the tip is placed over an area with low contact barrier [e.g., a grain boundary, position (2)], no spreading in the ZnTe occurs and only two terms remain: $R_{tot}(2) = R_t + R_c$.
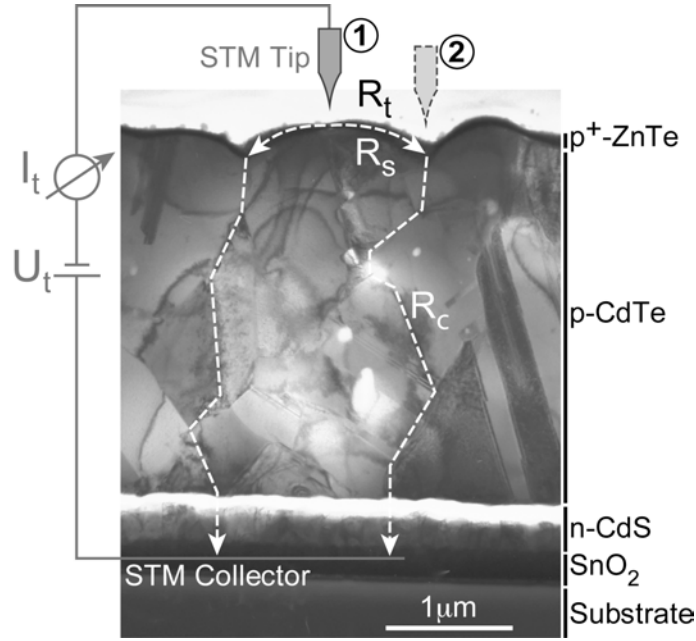
Fig. 3.1. XTEM cross-section of a p-CdTe/n-CdS solar cell.
The cell structure and the contact configuration used in STM measurements are shown.

Measuring, at constant tip-collector bias and as a function of tip position, the current injected into the cell should thus provide detailed maps of non-uniform carrier transport near the ZnTe/CdTe back contact interface. In particular, this technique should be sensitive to high-conductance pathways due to locally reduced contact resistance, e.g., at grain boundaries or in 'defective' grains. A relatively resistive contact layer (such as the ZnTe contact used here) is key for obtaining current contrast, since for a highly conductive (metallic) overlayer the spreading resistance $R_s(x,y)$ is small compared to the other resistance terms, thus providing negligible contrast. Other STM-derived techniques, such as ballistic electron emission microscopy have been developed to map the local height of potential barriers, e.g., at Schottky contacts on single crystal substrates. In comparison to this three-terminal technique, CIS is relatively simple and can be used to reliably map local contact resistances on complex polycrystalline photovoltaic devices.

Fig. 3.2 (a) shows a current map obtained at $U_t = 2V$ on a p^+-ZnTe capped p-CdTe/n-CdS solar cell. Dark (bright) shading in the image marks areas in which the current injected into the cell is low (high).
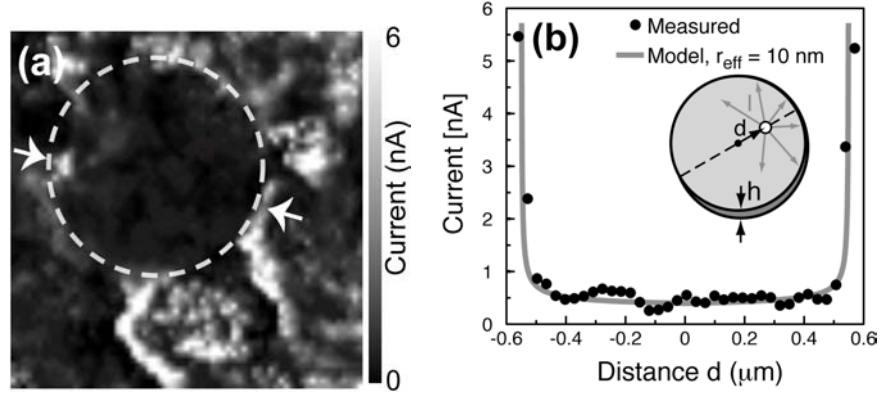
Fig. 3.2. Identification of the contrast mechanism in STM current maps on CdTe/CdS cells. (a) Grayscale STM current map at 2V bias (field of view: 2×2 μm^2). (b) Comparison of line profile across a single grain (between arrows in (a)) with model calculations for an effective injector radius of 10 nm. The inset illustrates the geometry assumed in the calculation.

The image shows substantial contrast in the form of large areas with uniformly low current, separated by bands of much higher conductance. We can use the data obtained on a single uniform grain (circle) and the surrounding grain boundary to verify the contrast mechanism proposed above, and to estimate the spatial resolution achievable in CIS. The expected current contrast due to a position dependent spreading resistance $R_s(x,y)$ was calculated for a simplified geometry of circular slab of ZnTe (thickness h) surrounded by a collector contact at its periphery (inset of Fig. 3.2 (b)). Current I injected at a distance d from the center of the slab will spread toward this collector contact. We have numerically computed the total resistance to current flow in the slab, as a function of the position and effective radius (r_{eff}) of the injector. The resulting current at constant injector-collector bias U_t was compared with the experimental data. For r_{eff} = 10 nm, we obtain excellent agreement between the computed and observed current distribution across a single grain. This result not only confirms the assumed contrast mechanism based on spreading in the ZnTe overlayer, but suggests that it should be possible to map preferential conducting paths near the absorber/contact interface with lateral resolution of about 20 nm.

Simultaneous measurements of sample topography and of current maps provide information on the spatial distribution of high conductance pathways at an ohmic contact to a solar cell, in our case at the p+-ZnTe/p-CdTe interface. A correlation of topography with current contrast is given in Fig. 3.3. Panels 3.3 (a) and (b) show the simultaneously measured

topography and current image within a field of view of $6 \times 6 \ \mu m^2$. The topographic scan [fig. 3.3 (a)] shows rounded elevated features, typically about 1.5 μm in diameter, separated by well-defined deep trenches. Based on comparison with XTEM, we associate the elevated areas with individual grains, and the intervening trenches with grain boundaries. The current map [fig. 3 (b)] shows large areas with roughly constant low current (dark), indicative of sample areas with low transmission probability across the ZnTe/CdTe interface, alternating with narrow, elongated conducting bands (bright) in which the contact is highly transparent.
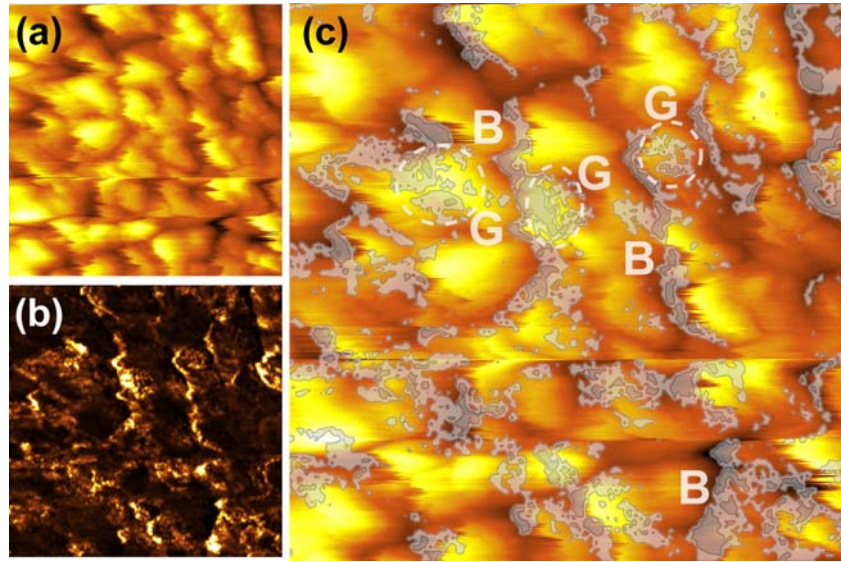

Fig. 3.3. (a) Topographic image obtained on a ZnTe capped CdTe/CdS cell (field of view: 6×6 μm^2, height scale: 0.7 μm). (b) Current map of the same region at 2V tip-collector bias (current range: $0 - 6 \ nA = I_{max}$). (c) Overlay of topographic data (color) with contours of the 2V current map. Light and dark gray areas, indicating current levels of 0.3 I_{max} and 0.85 I_{max}, respectively, trace troughs associated with grain boundaries (B) and some 'leaky' grains (G).

The position of these conducting paths is strongly correlated with grain boundaries. Fig. 3 (c) illustrates the correlation between topographic features and conductive pathways via a superposition of the topographic image with contours of constant current obtained from the current map. Regions of high current have a strong tendency to trace grain boundaries (B). The intragrain material generally shows rather uniform, low current, i.e., appears to be substantially more resisitive than grain boundaries. An exception are a few 'leaky' grains (G), in which a high density of microscopic conducting paths are observed.

Our data show substantial contrast on a nanometer length scale in the local transport properties of the p^+-ZnTe/p-CdTe interface of p-CdTe/n-CdS solar cells. The observed features appear unrelated to the grain structure of the small-grain ZnTe contact, but instead trace the topography of the underlying CdTe with its much larger grain size. This observation confirms that our data indeed map transport across the ZnTe/CdTe interface, and in the CdTe absorber near this interface. Current flow between absorber and back contact is highly non-uniform, with few low-resistance areas likely carrying a large fraction of the overall current of the cell. A majority of these areas trace grain boundaries, which indicates that grain boundaries may play a crucial role as conducting channels for carrier transfer into the cell back contact. Given that performance of polycrystalline CdTe/CdS solar cells is superior to single crystalline devices, a beneficial role of grain boundaries in carrier collection and transport, see e.g. [43, 11]. We provide the first observation of preferential current transfer into contacts via grain boundaries. Importantly, some intragrain material also shows efficient current transfer into the contact. Comparison with XTEM images suggests that structural defects or an accompanying segregation of impurities may be responsible for a local lowering of the contact barrier within some grains. This observation points toward a potential route for achieving substantial gains in cell efficiency via lowering of the back contact resistance by promoting these beneficial defects, and concomitant increases in short circuit current and fill factor.

3.2. New Experimental Capabilities

While the initial experiments discussed above involved local I-V measurements between ZnTe-capped CdTe/CdS cells in air, we have developed new experimental capabilities, direct conductance (dI/dV) mapping and imaging in high vacuum. These new capabilities will be discussed briefly below.

3.2.1. High-Resolution Conductance Mapping

We have developed the capability of obtaining, simultaneously with topographic images, conductance (dI/dV) curves on a regular grid within the image field of view. Similar to the I-V measurements, from which high-resolution current maps could be derived, the dI/dV data allow

us to produce maps of local conductance, dI/dV(x,y), near the back contact of a thin film solar cell. First results were obtained on a new batch of p^+-ZnTe capped p-CdTe/n-CdS solar cells with layout as shown in Fig. 3.1. Our previous measurements showed symmetric I-V curves, i.e., negligible rectification. In our new data, in contrast, a strong dependence of conductance on bias polarity (i.e., rectification) is observed, the origin of which requires further clarification. Fig. 4 shows representative conductance curves measured within a grain, and at a grain boundary of a device that has undergone CdCl$_2$ treatment and Br:MeOH etching prior to evaporation of thin Cu and ZnTe layers.
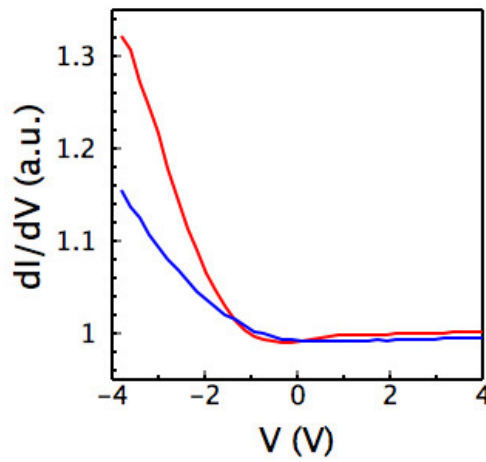

Fig. 3.4. Conductance spectra obtained at a grain boundary (red) and in intragrain material (blue). V > 0 corresponds to reverse bias of the main CdTe/CdS junction. Negative (positive) bias in fig. 4 corresponds to forward (reverse) bias of the p-CdTe/n-CdS junction of the cell.

We have obtained simultaneously measured maps of topography and local conductance, as shown in Fig. 3.5. The topographic image (Fig.3.5 (b)) shows, as before, rounded grains with diameter of about 1 μm, separated trenches that we identify as grain boundaries. The conductance map at positive bias (Fig. 3.5 (a)) shows the same general contrast distribution that was observed in current maps: high conductance preferentially near grain boundaries, uniform low conductance when the tip is placed over a grain. The conductance image at negative bias, however, deviates from this behavior. Instead of conducting paths near grain boundaries, we observe contrast that correlates much less with topographic features.
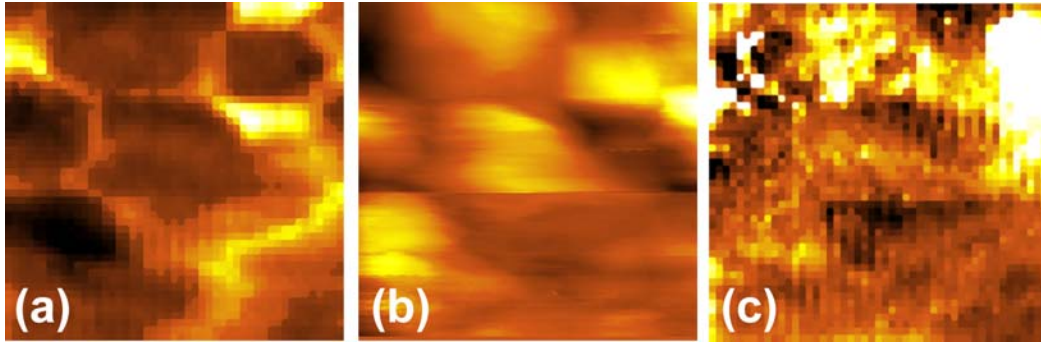
Fig. 3.5. Simultaneously measured topography and conductance maps (FOV: 2 × 2 μm).
a) dI/dV at V = +1 V (bright: high conductance). **(b)** Topography. **(c)** dI/dV at V = - 2.3V.

If we assume that the conductance images of Fig. 3.5 reflect high conductance pathways across the ZnTe/CdTe interface, we thus conclude that in these new devices clear differences exist between electron and hole transport across that contact. Currents of hole (majority carrier) injection into the CdTe are generally low, and strongly localized at grain boundaries. A substantial barrier to hole injection appears to exist at the contact to intragrain material. Electron injection, on the other hand, is more efficient and often shows minima at the grain boundary itself, surrounded by areas with higher conductance. A conclusive interpretation of these initial results of dI/dV maps requires additional measurements and modeling, and will be presented in the future.

3.2.2 Measurements in High- and Ultrahigh Vacuum

Most of the results shown above were obtained in a compact STM system, operating in air. Etched tungsten tips were generally used as probes for these measurements, since they can be formed into very sharp tips, required for scanning the rough surface of a solar cell. However, tungsten tips tend to oxidize over the extended times required to scan high-quality conductance maps. We have thus changed our experimental setup to be able to measure in high- or ultrahigh vacuum (Fig. 3.6). Incompatible materials, such as solder joints, were replaced with vacuum (UHV) compatible materials that can withstand baking temperatures up to 150°C required for rapid pump-down to UHV. In addition, we have implemented a heating system that will allow us

to anneal samples in vacuum, for surface cleaning, or to induce grain regrowth or impurity diffusion.

Fig. 3.6. Compact UHV STM system for imaging and spectroscopy on solar cell materials.

4. REFERENCES

1. S. Feldman, S. Townsend, R.T. Collins, V. Kaydanov, and T.R. Ohno. "Electroluminescence and Photoluminescence of Stressed and Unstressed CdTe/CdS Cells", *Proceedings of the NCPV Program Review Meeting*, September, 2001, Lakewood, CO.

2. W. Li, M. Ritala, M. Leskela, L. Niinisto, E. Spoinen, S. Sun, W. Tong, and C. J. Summers. "Photo- and electroluminescence of SrS:Cu and SrS:Ag,Cu,Ga thin films," *J. Appl. Phys*, **86** , 5017 (1999).

3. H. Song, X. Bao, N. Li, and J. Zhang, "Relation between electroluminescence and photoluminescence of Si^+-implanted SiO_2", *J. Appl. Phys.*, **82**, 4028 (1997).

4. M.V. Artemyev, V. Sperling, and U. Woggon, "Electroluminescence in thin solid films of closely packed CdS nanocrystals" *Appl. Phys.*, **81**, 6975 (1997).

5. N. L. Rowell, J.-P. Noel, S. C. Houghton, and M. Buchanan, "Electroluminescence and photoluminescence from $Si_{1-x}Ge_x$ alloys", *Appl. Phys. Letters*, **58**, 957 (1991).

6. V.G. Karpov, G. Rich, A.V. Subashiev, and G. Dorer, "Shunt Screening and size dependent effects in thin-film photovoltaics", *J. Appl. Phys*. **89**, 4975 (2001); V.G. Karpov, A.D. Compaan and Diana Shvydka, "Effects of nonuniformities in thin-film photovoltaics", *Appl. Phys. Lett* .**80**, 4256 (2002); V.G. Karpov, A.D. Compaan and Diana Shvydka, "Micrononuniformity effects in thin-film photovoltaics", Proc. *The 29th IEEE PVSC Conf.*, New Orleans, July 2002, p.708-711; V.G. Karpov, Diana Shvydka and A.D. Compaan "Nonuniformity Modeling and Taming", in *National CdTe R&D Team Meeting Minutes*, Golden, CO, July 10-11, 2003.

7. M. J. Romero, D. S. Albin, M. M. Al-Jassim, X. Wu, H. R. Moutinho, and R. G. Dhere, "Cathodoluminescence of Cu diffusion in CdTe thin films for CdTe/CdS solar cells", *Appl. Phys. Letters*, **81**, 2962 (2002).

8. S. A. Galloway, P. R. Edwards and K. Durose, "EBIC and cathodoluminescence studies of grain boundaries and interface phenomena in CdTe/CdS solar cells", *Inst. Phys. Conf. Ser.*, **157**, 579 (1997).

9. R. Harju, V. G. Karpov, D. Grecu, and G. Dorer, "Electron-beam induced degradation in CdTe photovoltaics", *J. Appl. Phys.*, **88**, 1794 (2000).

10. J. Hiltner, "Investigation of Spatial Variations in Collection Efficiency of Solar Cells". (*Ph.D. thesis*, Colorado State University, Fort Collins, CO), 2001.

11. M. K. Herndon, A. Gupta, V. Kaydanov, and R. T. Collins, "Evidence for the grain-boundary-assisted diffusion in polycrystalline CdS/CdTe heterojunctions", *Appl. Phys. Letters*, **75**, 3503 (1999).

12. D. Shvydka, A. D. Compaan, and V. G. Karpov, "Nonlocal response in CdTe photovoltaics", *J. Appl. Phys.*, **91**, 9059 (2002).

13. M. David, "Geostatistical Ore Reserve Estimation", Elsevier Scientific Publishing Co., Amsterdam, 1977, pp. 73-90.

14. A. S. Gilmore, V. Kaydanov, T. R. Ohno, D. Rose, S. D. Feldman, P. Erslev, "Treatment Effects on Deep Levels in CdTe Based Solar cells", *Proceedings of the 29th IEEE PV SC*, May, 2002, New Orleans, LA., p. 604.

15. A.D. Compaan, D. Shvydka, K.J Price, A. Vasko, and V.G. Karpov, "Bias-Dependent Luminescence in CdS/CdTe Cells", *Proceedings of the NCPV Program Review Meeting*, September, 2001, Lakewood, CO, pp.197-198.

16. Diana Shvydka, J.P. Rakotoniaina and O. Breitenstein, "Thermography. Mapping and Modeling", in *National CdTe R&D Team Meeting Minutes*", Golden, CO, July 10-11, 2003.

17. J. Tang, D. Mao, T. R. Ohno, V. Kaydanov, and J. U. Trefney, "Properties of ZnTe:Cu Thin Films and CdS/CdTe/ZnTe Solar Cells", *Proceedings of the 26th IEEE PV Specialists Conference*, October, 1997, Anaheim, CA, pp. 439-442.

18. D. Morgan, J. Tang, V. Kaydanov, T.R. Ohno, and J.U. Trefny, "Degradation Mechanisms Studies in CdS/CdTe Solar Cells with ZnTe:Cu Back Contact", *NCPV PV Progr. Review., Proc. 15th Conf.* , Denver, CO, September 1998, pp. 200-205.

19. D. Grecu and A. D. Compaan, "Photoluminescence study of Cu diffusion and electromigration in CdTe", *Appl. Phys. Lett.* **75**, 361 (1999); D. Grecu, A. D. Compaan, D. Young, U. Jayamaha and D. H. Rose, "Photoluminescence of Cu-doped CdTe and related stability issues in CdS/CdTe solar cells", *J. Appl. Phys.* **88**, 2490 (2000).

20. Kenneth Zanio, "Semiconductors and Semimetals, Volume 13, Cadmium Telluride", *Academic Press, New York, San Francisco, London*, Copyright © 1978, p.148

21. A. Balcioglu, "Characterization of Deep Impurity Levels in Semiconductor Devices", Ph.D. Thesis, Colorado School of Mines, Golden, CO, 2001.

22. S.-H. Wei "Role of Defects and Grain Boundaries on Stability", in *National CdTe R&D Team Meeting Minutes*", Golden, CO, January 25-26, 2001.

23. A.S. Gilmore, V. Kaydanov, T.R. Ohno, and D. Rose, "Admittance Spectroscopy of Deep Levels in CdTe Solar Cells", *NCPV Progr. Rev. Meeting 2001*, Oct. 2001, Laikewood, CO, pp. 199-200.

24. P. Nollet, M. Burgelman, S. Degrave, and J.Beier, " Importance of Air Ambient during CdCl$_2$ Treatment of Thin Film CdTe Solar Cells Studied through Temperature Dependent Admittance Spectroscopy", *Proceedings of the 29th IEEE PV SC*, May, 2002, New Orleans, LA., pp. 704-707.

25. D. Shvydka, U. Jayamaha, V.G. Karpov, and A.D. Compaan, "Capacitance-Frequency Analysis of CdTe Photovoltaics", *ibid.*, pp. 752-755.

26. A.S. Gilmore, V. Kaydanov, T.R. Ohno, "The Study of Deep Levels in CdS/CdTe Solar Cells Using Admittance Spectroscopy and its Modifications", *MRS Spring 2003*, S. Francisco, CA, April 2003, pp.

27. P. Blood and J.W. Orton, "The Electrical Characterization of Semiconductors: Majotity Carriers and Electron States", ACADEMIC PRESS, *Harcout Brace Jovanovich, Publishers, London - San Diego - New York – Boston – Sydney – Tokio – Toronto*, Copiright ©1992.

28. V. Kaydanov, "Capacitance/Conductance Spectroscopy of Deep States and Hole Concentration in CdTe Solar Cells", in *National CdTe R&D Team Meeting Minutes*", Golden, CO, Oct. 31-Nov. 01, 2002.

29. T. Walter, R. Herberholz, C. Muller, and H.W. Schock, "Determination of defect distributions from admittance measurements and application to Cu(In,Ga)Se$_2$ based heterojunctions", *J. Appl. Phys.* **80**, 4411 (1996).

30. C.E. Michelson, A.V. Gelatos, and J.D. Cohen, "Drive-level capacitance profiling: Its application to determining gap state densities in hydrogenated amorphous silicon films", *Appl. Phys. Lett.* **47**, 412 (1985).

31. L.C. Kimmerling, "Influence of deep traps on the measurement of free-carrier distributions in semiconductors by junction capacitance techniques" *J. Appl. Phys.* **45**, 1839 (1974).

32. R.A. Sasala and J.R. Sites, "Transient Voltage of Thin-film Polycrystalline Solar Cells", *AP. Conf. Proc.* 268 , *PV Advanced R&D Project*, Denver, CO, 1992, pp.218-227.

33. R.A. Sasala and J.R. Sites, "Time –Dependent Voltage in CuInSe$_2$ and CdTe Solar Cells", *Proc. 23d IEEE PVSC,* p.543 (1993).

34. T.J. MacMahon, "Dark Curernt Transients in Thin-Film CdTe Solar Cells", *Proceedings of the 29th IEEE PV SC*, May, 2002, New Orleans, LA., pp. 768-771.

35. S. W. Johnston, R.S. Crandall, "Evidence of the Meyer-Neldel Rule in InGaAsN alloys: Consequences for Photovoltaic Materials", *MRS Spring 2003*, S. Francisco, CA, April 2003. (Additional data and analysis can be found in the Poster presented by the authors).

36. D.L. Young, K. R. Ramanathan, M. Contreras, J. Abushama, R. S. Crandall, "A Barrier To Trap Filling in CuIn$_{1-x}$Ga$_x$ Se$_2$", *Ibid*.

37. R.S. Crandall, *J. Electron. Mat.*, 9, 713 (1980)

38. L.M. Woods, D.H. Levi, V. Kaydanov, G.Y. Robinson, and R.K. Ahrenkiel, "Electrical Characterization of CdTe Grain-Boundary Properties from As Processed CdTe/CdS Solar Cells", in *Proc. 2nd World Conf. on PV Solar Energy Conversion*, July 1998, Vienna, Austria, pp. 1043-1046; "Electrical Characterization of Etched Grain-Boundary Properties from As-Processed p-CdTe Based Solar Cells", *Proc. NCPV PV Progr. Rev. Meeting*, Denver, CO 1998, AIP CP462, pp.499-504.

39. A.S. Gilmore, V. Kaydanov, U. Laor, T.R. Ohno, B. McCandless, " AC Characterization of Grain Boundary Electronic Properties in CdTe Thin Films", *Proc. NCPV Progr. Rev. Meeting 2000*, Denver, CO, April 2000, pp.259-260.

40. V.I Kaydanov and T.R. Ohno, "Process Development and Basic Studies of Electrochemically Deposited CdTe-Based Solar Cells", Final Technical Report, 15 May 1988-17August 2001, NREL/SR-520-31777, Colorado School of Mines, March 2002.

41. J.H. Scofield, "Effects of series resistance and inductance on solar cell admittance measurements", *Solar Energy Materials and Solar Cells* **37**, 217 (1955).

42. I. Visoly-Fisher, S.D. Cohen, D. Cahen, "High Resolution Characterization of a Single Grain Boundary in CdTe/CdS Solar Cells", *MRS Spring 2003*, S. Francisco, CA, April 2003, pp. ,

43. V. Kaydanov, "Some Possible Effects of Grain Boundaries on Thin Film Cell Performance", In "*National CdTe R&D Team Meeting Minutes*", Golden, CO, January 27-28, 2000; Appendix 33.

5. ACKNOLEDGEMENTS

Many people, in addition to those at the Colorado School of Mines, have contributed to this work over the past year.

We are thankful to Peter Meyers and Anke Abken of First Solar, LLC., for supplying us with the materials for the CdTe/Cells preparation at our facilities and also the completed cells (stressed and unstressed) for studies.

We appreciate greatly possibility to cooperate with our partners in the National CdTe R&D team: Prof. J. Sites, T. Nagel, Prof. W. Sampath et. al (Colorado State University); Prof. A. Compaan, Prof. V. Karpov, Dr. D. Shwydka et al. (University of Toledo); Dr. D. Albin (NREL), Prof. C. Ferekides (university of S, Florida)

It is hard to underestimate the value of discussions of our research approach and results that we have had with the individuals mentioned above and also Alan Fahrenbruch, Bolko von Roedern, Tim Gessert, Brian McCandless, R. Crandall, D. Young, S. Johnston and other scientists involved in fabrication and studies of thin film solar cells.

We greatly appreciate the encouraging interest in our activities, visiting our facilities, discussions and suggestions we receive from the management of Thin Film Partnership Program: Kenneth Zweibel (who is also our subcontract technical monitor), Bolko von Roedern and Harin Ullal.

6. APPENDICES

6.1 Personnel

The names, titles, and representative responsibilities of the individuals contributed to this work are summarized below.

Timothy R. Ohno, Associate Professor of Physics: Photovoltaic Development, Surface Physics, Electroluminescence, Principal investigator

Victor I. Kaydanov, Research Professor of Physics: Photovoltaic Development, Electron Transport , Studying of the Defect Electronic States, Principal Investigator

Reuben T. Collins, Professor of Physics: Electronic and Optical Properties of Semiconductors, NSOM, Photo- and Electroluminescence

Colin Wolden, Associate Professor of Chemical Engineering: JVD System Design

Peter Sutter, Associate Professor: Scanning Tunneling Microscopy and Spectroscopy

Eli Sutter, Assistant Professor: Transmission Electron Microscopy

Joe Beach, Post. Doc. Fellow: Cell Processing and Characterization

Angelo S. Gilmore, Graduate Research Assistant, then Post. Doc. Fellow: Admittance Spectroscopy, Hall effect.

Scott Feldman, Graduate Research Assistant: Cell Electroluminescence and Photoluminescence, Micrononuniformity

James Kestner, Graduate Research Assistant: Developing of JVD System, Cell Processing

Fred Seymour, Graduate Research Assistant: Studying of deep electronic states by means of admittance spectroscopy and transients; Developing of Data Base

Sean Gooding, Undergraduate Research Assistant: Characterization, Equipment Construction

6.2   Publications

1. A. S. Gilmore, V. Kaydanov, T. R. Ohno, D. Rose, S. D. Feldman, P. Erslev, "Treatment Effects on Deep Levels in CdTe Based Solar cells", *Proceedings of the 29th IEEE PV SC*, May, 2002, New Orleans, LA., p. 604.

2. A.S. Gilmore, V. Kaydanov, T.R. Ohno, "The Study of Deep Levels in CdS/CdTe Solar Cells Using Admittance Spectroscopy and its Modifications", *MRS Spring 2003*, S. Francisco, CA, April 2003.

3. S.D. Feldman, T.R. Ohno, V. Kaydanov, and R.T. Collins, "Development of Electroluminescence Imaging Characterization for CdS/CdTe Solar Cells", *Ibid.*

4. J.M. Kestner, Sarah McElvain, and Colin Wolden, "Vapor Transport Deposition and Characterization of Polycrystalline CdTe Solar Absorbers", *Ibid.*

5. S.D. Feldman, F.H. Seymour, T.R. Ohno, V. Kaydanov, and R.T. Collins, "Development and Application of Electroluminescence Imaging for CdS/CdTe Solar Characterization", *NCPV and Solar Progr. Rev. 2003*, Denver, CO, March 24-26, 2003.

6. J. Kestner, S. McElvain. C.A. Wolden, T. Ohno, and Lawrence Woods, " Temperature Dependence of Growth Rate and Morphology of Vapor Transport Deposited CdTe Thin Films", *Ibid.*

6.3   Presentations

1. S.D. Feldman, T.R. Ohno, V. Kaydanov, R.T. Collins, "Electroluminescence Studies", in *"National CdTe R&D Team Meeting Minutes"*, Golden, CO, Oct. 31-Nov. 01, 2002, Appendix 8.

2. V. Kaydanov, "Capacitance/Conductance Spectroscopy of Deep States and Hole Concentration in CdTe Solar Cells", in *"National CdTe R&D Team Meeting Minutes"*, Golden, CO, Oct. 31-Nov. 01, 2002, Appendix 32

3. S.D. Feldman, ", T.R. Ohno, V. Kaydanov, and R.T. Collins, "Back Contact Nonuniformity Studied with Luminescence Technique", in *"National CdTe R&D Team Meeting Minutes"*, Golden, CO, July 10-11, 2003, Appendix 6

4. P. Sutter, P. Zahl, E. Sutter, V. Kaydanov, T. Ohno, "High-Resolution Electron Structure Mapping on Polycrystalline CdTe Solar Cells by Scanning Tunneling Microscopy", *MRS Spring 2003*, S. Francisco, CA, April 2003.